CRISTA observations of cirrus clouds around the tropopause

Reinhold Spang,[1] Gunnar Eidmann, Martin Riese, Dirk Offermann, and Peter Preusse
Department of Physics, University of Wuppertal, Wuppertal, Germany

Leonhard Pfister
NASA/Ames Research Center, Moffett Field, California, USA

Pi-Huan Wang
Science and Technology Corporation, Hampton, Virginia, USA

Received 29 March 2001; revised 15 August 2001; accepted 16 August 2001; published 6 September 2002.

[1] The Cryogenic Infrared Spectrometers and Telescopes for the Atmosphere (CRISTA) instrument observed thin cirrus clouds at and above the tropopause during its two missions in November 1994 and August 1997. A simple cloud detection scheme was developed for extinctions greater than 2×10^{-3} km^{-1} through analysis of the measured infrared spectra in the 12-μm range. Horizontal and vertical distributions of cloud occurrence frequencies are in good agreement with the Stratospheric Aerosol and Gas Experiment (SAGE) II subvisual cirrus cloud (SVC) climatology as well as SAGE measurements for the 1997 period. Seasonal variations, strong longitudinal variability, and indications of enhanced cloud occurrence frequencies in separated regions caused by El Niño events were detected in the CRISTA data set. A substantial day-to-day variability could be found throughout the tropics, and several regions with enhanced variability have been identified. In addition, a significant amount of cloud was found above the midlatitude tropopause. Backward trajectories in relation to outgoing longwave radiation (OLR) measurements and cloud observation in the troposphere by meteorological satellites suggest that about three fourths of the high clouds (>15 km) observed by CRISTA in the tropics stem from deep convection systems and the outflow of these systems. This would imply that on the order of at least one fourth of the observed cloud events are originated by other mechanisms, such as in situ formation due to cooling events on synoptic and/or gravity wave scales. For the convective generated cirrus clouds, a maximum lifetime of around 3–4 days was estimated over a wide range of latitudes. Such a long lifetime could be important for modeling the impact of cirrus clouds on radiation budget (climate) and heterogeneous chemical processes around the tropopause. *INDEX TERMS:* 0320 Atmospheric Composition and Structure: Cloud physics and chemistry; 3314 Meteorology and Atmospheric Dynamics: Convective processes; 3360 Meteorology and Atmospheric Dynamics: Remote sensing; 3362 Meteorology and Atmospheric Dynamics: Stratosphere/troposphere interactions

Citation: Spang, R., G. Eidmann, M. Riese, D. Offermann, P. Preusse, L. Pfister, and P.-H. Wang, CRISTA observations of cirrus clouds around the tropopause, *J. Geophys. Res.*, *107*(D23), 8174, doi:10.1029/2001JD000698, 2002.

1. Introduction

[2] Cirrus clouds at and around the tropopause play an important role in different fields of atmospheric studies. Cirrus clouds significantly impact the radiation budget due to the absorption of outgoing longwave radiation (OLR) and emission at the very low tropical tropopause temperature [*Jensen et al.*, 1996a], whereby the radiative forcing of the climate system is modified [e.g., *Sassen et al.*, 1989]. If air rises across the tropopause the formation of cirrus cloud particles could potentially limit the amount of water vapor entering the stratosphere [*Danielsen*, 1993] and would act like a fingerprint of the stratospheric dehydration mechanism. Heterogeneous chemical reactions on cirrus particles around the tropopause can lead to effective and rapid ozone destruction [*Borrmann et al.*, 1996], which may partly generate the unusually large ozone trends around the midlatitude tropopause region [*Solomon et al.*, 1997]. How the formation of cirrus clouds around the tropopause works is still unclear. Two favored mechanisms are under discussion: (1) dissipation of cumulonimbus outflow anvils in deep convection systems leaves behind an optically thin layer of

[1]Now at EOS, Space Research Centre, University of Leicester, England, UK.

0148-0227/02/2001JD000698

small ice particles [*Danielsen*, 1993] and (2) in situ nucleation of ice crystals by homogeneous freezing of sulfuric acid aerosols due to uplift and cooling of a humid layer on both a synoptic and a gravity wave scale [*Jensen et al.*, 1996b].

[3] Cirrus clouds can affect remote sensing measurements through enhanced absorption and emission. Around the tropopause cirrus clouds are frequently optically thin and not detectable in the visible or reported by ground based weather observers. These clouds are very difficult to observe especially for nadir-looking instruments and are often described as subvisual cirrus clouds (SVC) following the classification scheme by *Sassen and Cho* [1992]. The horizontal and vertical extension may be very variable. The Lidar in Space Technology Experiment (LITE) [*Winker and Trepte*, 1998] detected so-called laminar cirrus often above or downstream of convective systems with a horizontal extent from <100 km up to 2700 km and thickness of less than 200 m in an altitude region of 14 to 18.7 km. The persistence of cirrus clouds (cloud lifetime) around the tropopause is important for the quantization of the radiative effect [*Jensen et al.*, 1996a], though little is known from observations for that purpose.

[4] In the 1980s and 1990s several remote sensing instruments from space investigated the detection of cirrus clouds on a near global basis. *Prabhakara et al.* [1993] found that the seasonal average cloud cover produced by thin cirrus is as large as 50% over the tropical western Pacific. This analysis was restricted to areas above sea surface only and was made by the nadir-looking Infrared Interferometer Spectrometer (IRIS) on Nimbus 4. First global analyses of optically very thin clouds has been provided by the limb-viewing occultation observations of the Stratospheric Aerosol and Gas Experiment (SAGE) II [*Wang et al.*, 1994], complemented by more recent experiments of the Upper Atmosphere Research Satellite (UARS) [*Hervig and McHugh*, 1999; *Mergenthaler et al.*, 1999]. The most complete and reliable data set describing the seasonal variability and geographical distribution of SVCs by the SAGE II data was presented by *Wang et al.* [1996].

[5] This paper presents a somewhat complementary data set obtained from observations of the Cryogenic Infrared Spectrometers and Telescopes for the Atmosphere (CRISTA) experiment. The studies are presented in the following manner: After a brief description of the CRISTA instrument, section 3 will introduce the cloud detection method in detail. Section 4 gives an overview of the global cloud observations around the tropopause for both missions. Comparisons with the SAGE II climatology and 1997 measurements of SVCs on a zonal mean basis as well as longitude–latitude distributions will be presented, followed by an analysis of the cloud top temperature in section 5. The combination of the CRISTA cloud events with backward trajectory analyses and cloud observations by meteorological satellites will be used in section 6 to give evidence for the formation mechanism and origin of the clouds observed by CRISTA.

2. The CRISTA Instrument

[6] CRISTA is a limb-scanning instrument, which measures the thermal emission of 18 trace gases in the 4–71 μm range [*Offermann et al.*, 1999; *Riese et al.*, 1999a]. The instrument is especially designed for high spatial resolution in all three dimensions by using three telescopes looking 18° horizontally apart. The optics and the infrared detectors are cooled by cryogenic helium. This results in high sensitivity of the detectors and the IR spectra being scanned very fast (4–15 μm in 1.2 s), which consequently yields a high spatial resolution. One of the main scientific objectives of CRISTA is to detect small scale dynamically induced structures in the temperature and trace gas distributions of the middle atmosphere [*Offermann et al.*, 1999; *Riese et al.*, 1999b]. However, CRISTA is also suitable for the study of specific cloud features around the tropical tropopause as well as in the cold stratospheric polar vortex by means of the information content of the measured spectra.

[7] The instrument was flown in space twice (on the NASA Space Shuttle) for a measurement period of around one week in November 1994 (5–12) [*Offermann et al.*, 1999] and August 1997 (8–16) [*Grossmann et al.*, 2002]. During the missions CRISTA was integrated in the free-flying satellite ASTRO-SPAS. For the first flight the latitudinal coverage was 57°S–64°N. Due to the pointing capabilities of the ASTRO-SPAS system the coverage was extended to 74°S–74°N for the second mission by slewing the satellite (57° orbit inclination) at high northern latitudes to the north and at southern latitudes to the south.

[8] In the tropics a horizontal resolution was achieved of around 200–400 km along the orbit track and 600 km cross track respectively. The resulting dense measurement net allows high quality occurrence statistics for clouds in spite of the short measurement periods of only one week. The sample volume has a length along the view direction of roughly 280 km and a sample volume width across the view direction of around 20 km. The vertical field of view is on the order of 1.5 km. One tilting mirror for each telescope realizes the altitude scan through the atmosphere. For CRISTA-1 an altitude step spacing of 1.5 km has been applied, and 2 km for the second mission. For the derived tangent heights over the Earth ellipsoid, an accuracy on the order of ±300 m or better and a precision of ±80 m has been achieved by the post flight attitude processing [*Offermann et al.*, 1999]. The vertical resolution is on the order of 2.0 km [*Riese et al.*, 1999a].

3. Cloud Detection Method

[9] For the detection of clouds a simple but robust cloud-free indicator (CI) was developed by means of the CRISTA spectral measurements. Figure 1 shows the limb radiance spectra in the 700–1650 cm^{-1} region for cloudy (black) and noncloudy (gray) conditions in the tropics at around 17 km. The spectral resolution ($\lambda/\Delta\lambda$) is on the order of 500. The spectral coverage is not continuous but includes some gaps resulting from the instrument design. Tremendous intensity changes could be observed, when the instrument looks into a cloudy region. The enhanced radiation by clouds produces a significant change in the spectral shape, especially in the wave number regions 800–950 cm^{-1} and 1150–1250 cm^{-1}. Parts of these wave number regions act as atmospheric windows for clouds and aerosols, because only few gases with low emissions are present. The enhanced radiation by clouds in the 840–860 cm^{-1} range, where CFC11

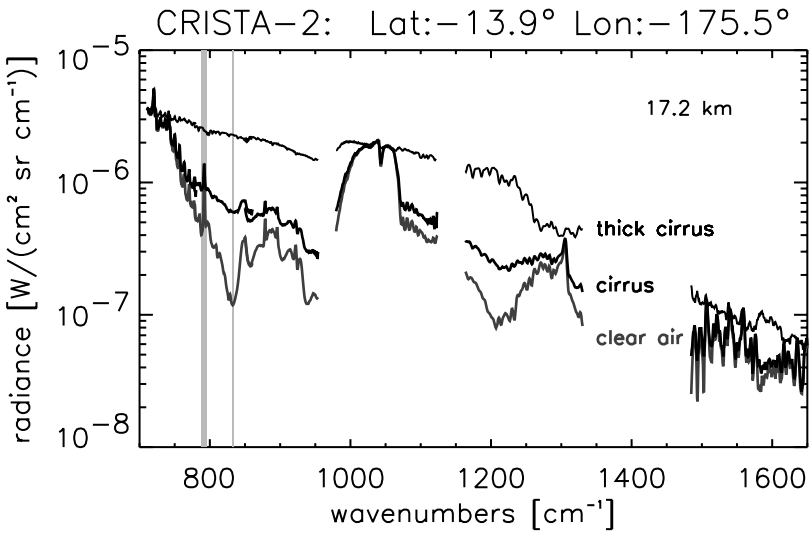

Figure 1. Three single spectra in the tropical tropopause region for clear air (gray thick curve), optically thin (black thick curve), and optically thick conditions. Clear air and thin cirrus spectra are measured at 17.2-km altitude in two subsequent profiles around 300 km apart. The optically thick spectrum represents a measurement 2 km below the optically thin case. The wave number regions for the defined CI are indicated by gray vertical bars.

is also a strong emitter, has been previously reported by *Spang et al.* [1997] for the CRISTA-1 mission. In the present study, the cloud detection is accomplished by using the ratio of radiances in the 788–796 cm^{-1} CO_2 dominated and the 832–834 cm^{-1} aerosol dominated wave number regions (Figure 1, gray-shaded areas). The latter region contains only weak emissions of ozone and CFC11 in comparison to the background aerosol and the enhanced cloud emissions. In the following the defined ratio will be referred to as the CI.

[10] Sensitivity studies for CI with the CRISTA forward radiance model [*Riese et al.*, 1999a] were carried out using extreme atmospheric constituent and temperature profiles [*Remedios*, 1999]. The analysis shows that in the height regime 12–40 km a ratio of CI = 2 or smaller can only be produced by a radiation background anomalously enhanced by aerosols or clouds. The temperature dependence of CI is especially weak (<1% K^{-1} in the 10 to 30 km range). Figure 2 shows a tropical cloudy and a noncloudy CRISTA height profile of CI. The enhanced radiation in the aerosol channel (see also Figure 1) causes the values of the measured cloudy profile (thick black line) to shrink to values below 2 over two height steps (18 to 16 km) in comparison to values CI > 4 for the noncloudy profile. The influence of aerosol/cloud radiation starts normally at values around 3–4. Such values can be created by very thin clouds or if the cloud does not completely fill the field of view of the CRISTA instrument (1.5 km). The distinction between these two cases is very difficult to define and is not considered in the following analyses. Many of the cloud influenced height profiles become optically thick in an altitude layer below the first cloud indications, and this is indicated by the nearly constant CI values below 14 km (Figure 2).

[11] Spectra with CI $\leq$ 2 are not necessarily optically thick as shown in Figure 1. For optically thick conditions the spectral shape adopts a gray or blackbody curve and additional scattering effects occur, which also produce a strong background radiation leading to small CIs. The radiance emanating toward an IR limb scanner instrument (12.8 μm) can be enhanced by scattering for example by 25% for 0.8-μm-radius ice particles near the tropical tropopause over a 300 K surface (tropical ocean) [*Mergenthaler et al.*, 1999]. The enhancements increase for larger particles. Therefore CI works also like an indicator for scattered radiation by clouds. So far scattering effects are not able

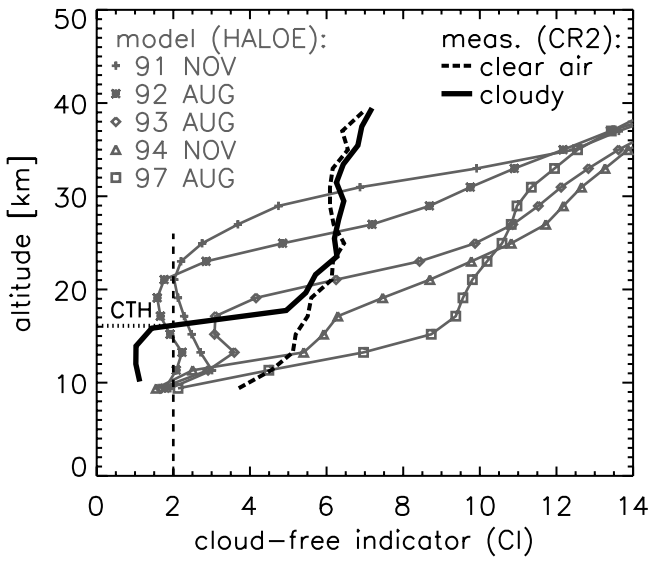

Figure 2. Comparison of simulated (gray) CI profiles using the CRISTA forward radiance model and measured profiles (black thick/dash-dotted for cloudy/clear air conditions). Simulations are performed for different aerosol loadings (symbols) using HALOE 5.26-μm extinction values and CRISTA-2 mean constituent profiles for tropical conditions.

to consider in a retrieval in the infra red and the error for any retrieved extinction would be large if clouds are in the line of sight. In addition a background radiation problem (presumably stray light) in the CRISTA instrument gets increasingly significant above 20 km producing excessive radiances in the aerosol channel (enumerator of CI). This implies overestimated and roughly constant CIs above 25 km, where normally the aerosol radiances decrease rapidly (Figure 2). This problem also hampers a detailed retrieval of aerosol extinction profiles. Retrieval studies show that a CI threshold of 2 corresponds to extinctions on the order of 2×10^{-3} to 5×10^{-2} km^{-1}. Unfortunately the large uncertainty in extinction makes it impossible to determine the visible optical depth or the emissivity of the clouds. Therefore it is not possible to quantify the radiative effect of the observed clouds. In summary we have used CI and not extinction profiles for the cloud indication because the characteristic change in the spectral shape of the measured spectra is the most sensitive indicator for clouds in the line of sight of the instrument.

[12] To investigate how accurately clouds can be distinguished from enhanced background aerosol, the sensitivity of CI was tested for different aerosol loadings using extinction measurements of the Halogen Occultation Experiment (HALOE) on the Upper Atmospheric Research Satellite (UARS). Mean tropical extinction profiles of the version 19 data set of the 5.26 μm channel were computed for the forward calculations (Figure 2). Measurements and forward model calculations show quite different gradients for CI > 5 caused by the CRISTA straylight problem mentioned above. But in the area of interest (<25 km) forward calculation and measurement can compare with each other. The CRISTA measurements happened under the condition of low stratospheric aerosol loading for CRISTA-1 and especially very low loading for CRISTA-2 [*Thomason and Poole*, 1999]. This is seen in the November 1994 and August 1997 forward calculations (CI > 4 above 12 km). The strongly enhanced aerosol loading by the Mount Pinatubo eruption in 1991 is indicated by very low CIs in the lower and middle stratosphere for the years 91, 92 and even 93. It is well known that the detection of optically thin clouds is quite difficult in the post-Pinatubo eruption period [e.g., *Wang et al.*, 1996]. However, as Figure 2 demonstrates the cloud detection scheme works very well during the two CRISTA periods and the criterion CI < 2 is proved to be a conservative and robust threshold.

[13] The analysis also allows a rough *cloud top height* (CTH) to be defined by computing the first tangent height where the CI falls below the specified threshold of CI < 2 (Figure 2) during a downward scan. The CTHs were used for the computation of cloud occurrence frequencies f_c by the following expression:

$$f_c(i) = \frac{N_c(i)}{N(i) - \sum_{i+1}^{n} N_c(i)} \times 100 \quad [\%]$$

where $N(i)$ indicates the total number of CRISTA overpasses in a defined latitude–longitude grid box at altitude level $z(i)$, with $I = 1 \ldots n$ from the bottom to the top level of the analysis. $N_c(i)$ is defined by the number of cloud events $N_c(i)$ (detected CTHs) in the layer i. By the definition of CI and CTH it is not possible to detect clouds underneath the first detected cloud layer in a height profile. Therefore it is necessary to diminish $N(i)$ for the analysis by all cloud observations in the layers above ($\sum_{i+1}^{n} N_c(i)$).

4. Global Cloud Top Distribution

[14] For the determination of cloud properties and statistics the handicap of shortness of the CRISTA missions was partly compensated by the unprecedented density of measurements. The total number of profiles for both missions is comparable to a measuring period of around 7 years for an occultation experiment. The global CRISTA-2 distribution of all detected CTHs above 8 km are presented in Figure 3. Each symbol represents an individual CTH location in the CI profiles. The highest CTH are plotted on top, therefore partly lower CTHs are hidden. Noncloudy regions between 74°S and 74°N are indicated by open areas (no data gaps). More than one third of the total number of 43000 radiance profiles is affected by clouds. During the first mission considerably less CTHs have been detected (17% of 50000 profiles, not shown). This is because the minimum tangent height of an altitude scan was on the order of 14–15 km compared to 8–10 km for CRISTA-2 for instrumental reasons.

[15] A belt of high clouds could be observed in the tropics (CTH > 16 km) especially in the monsoon area over North India with CTH up to 18 km, where deep convection can penetrate into the lower stratosphere during this season (NH summer). Obviously the subtropics are an area of reduced cloud activity, indicated in Figure 3 by cloud-free regions, for example over Australia, parts of the Pacific and Atlantic. The midlatitudes show a higher activity and CTH up to 14 km (significantly above the tropopause). The computation of CI and CTH are also useful for the detection of polar stratospheric clouds (PSC). Due to the large latitudinal coverage (±74°), CRISTA-2 made observations deep inside the south polar vortex for midwinter conditions and most of the cloud detections southward of 60° show CTHs (up to 24 km) which originate from the formation of PSC in the cold lower stratosphere of the Antarctic polar vortex [*Spang et al.*, 2001].

4.1. Zonal Mean Occurrence Frequencies

[16] The zonal mean distribution of cloud occurrence frequencies of the CRISTA-2 CTHs is displayed in Figure 4 in comparison to the SAGE II seasonal mean of subvisual cloud frequencies from June to August 1997. For the CRISTA analysis a latitude height grid of 5° × 1 km was used in comparison to a 10° × 1 km grid for SAGE II. Despite the difference in data period (3 month/1 week), both statistics look very similar, with maxima in the tropics around the tropopause, local minima in the subtropics (in the NH more significant for CRISTA), and increasing frequency around the midlatitude tropopause. The absolute values are generally somewhat smaller for CRISTA than for SAGE II. In particular, SAGE II observed significantly more clouds above the tropical tropopause. This discrepancy is presumably partly caused by the different detection schemes.

[17] The SAGE II cloud analysis corresponds to a range of 1.02 μm extinction coefficients from 2×10^{-4} km^{-1} to 2×10^{-2} km^{-1}. Following the cirrus cloud classification of *Sassen and Cho* [1992], this range of extinction coefficients corresponds to subvisual clouds. For clouds with extinction

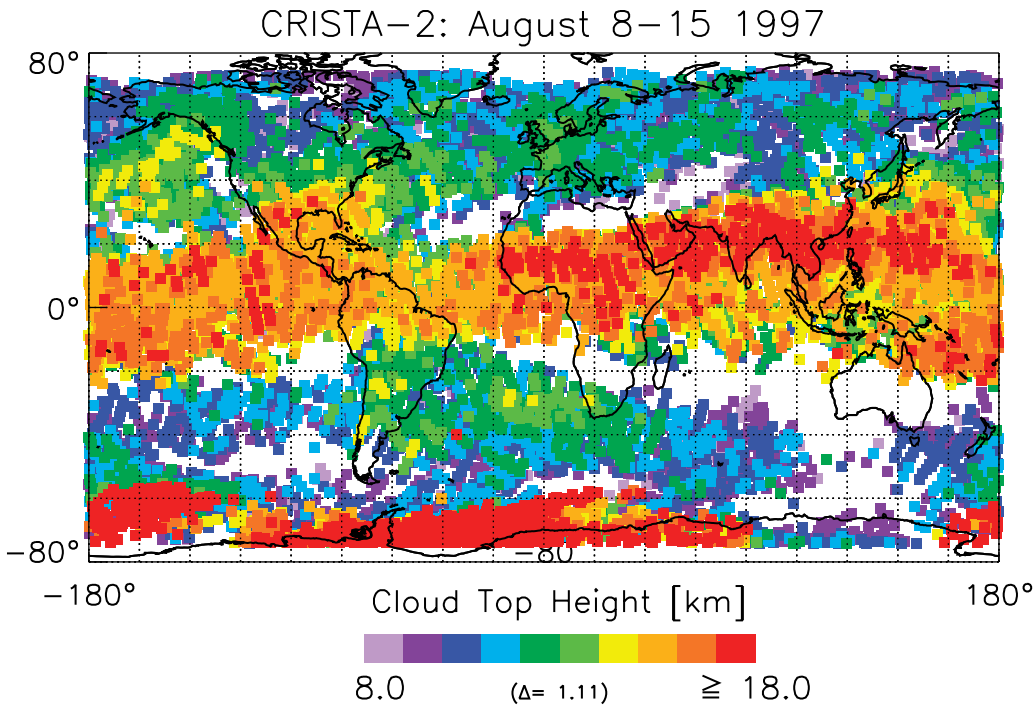

Figure 3. CRISTA-2 global map of the CTHs detected by the cloud identification scheme. Latitude range is −80 to +80 and time interval is 8–15 August 1997.

coefficients greater than 2×10^{-2} km^{-1}, they are referred to as SAGE II opaque clouds [*Wang et al.*, 1996]. This compares to the rough extinction threshold for CRISTA of 2×10^{-3} km^{-1} at 12.0 μm. To relate these different thresholds in the two wavelength regions model calculations with a classical Mie code would be necessary. *Mergenthaler et al.* [1999] realized this for cloud analyses using the UARS-CLAES 12.8 μm extinction data in relation to SAGE II. The CLAES and CRISTA wavelength regions are very close to each other. On a qualitative basis it is permissible to transfer the CLAES/SAGE comparison to CRISTA/SAGE. Mergenthaler et al. figured out that the SAGE II cirrus classification should include much thinner clouds, because the CLAES extinction threshold (9×10^{-4} km^{-1}, which is very close to the lower CRISTA limit of 2×10^{-3} km^{-1}) corresponds to 8–35 times larger extinctions at 1.02 μm than the SAGE threshold. The variability is given by the particle size dependence, where large extinctions are produced by large ice crystals. Consequently the estimated CRISTA extinction range for CI is also less sensitive than the SAGE extinction criterion. The lower occurrence frequencies above the tropopause and the lower altitude for the maximum of the zonal mean occurrence distribution in the tropics in comparison to SAGE may be affected by this circumstance. In addition the CRISTA cloud detection scheme cannot distinguish between subvisual and opaque clouds. Opaque clouds become the dominant cloud type in the midlatitudes below 10 km in the SAGE climatology and are not included in SAGE II statistics of SVCs in Figure 4b.

4.2. Seasonal and Longitudinal Variations

[18] Latitude–longitude distributions of the cloud occurrence frequencies for CRISTA-1 (17.5 km) and CRISTA-2 (13.5, 15.5 and 17.5 km) in comparison to the SAGE II climatology for SVCs [*Wang et al.*, 1996] are presented in Figures 5 and 6. The CRISTA statistics are based on a longitude–latitude height grid box of 24° × 10° × 1 km, which is the same gridding as in the SAGE analyses. As mentioned above, the minimum tangent height during CRISTA-1 was 15.5 km whereby only the 17.5 km level for CRISTA-1 can be compared with the climatology. The climatology is based on a six year mean of three month periods of the SAGE II measurement period 1985–1990 [*Wang et al.*, 1996], September to November for CRISTA-1 and June to August for CRISTA-2. For CRISTA-1 the clouds occur most frequently over south America, central Africa, and the Indonesia/Micronesia region, all of which are areas of convective activity. For CRISTA-2 (15.5 km) all maxima are shifted more to the north, due to the northern hemisphere summer conditions and the implicit north shift of the intertropical convergence zone (ITCZ).

[19] The CRISTA-1 cloud statistics show excellent agreement for the location of the cloud activity centers in comparison to the SAGE climatology. However, the CRISTA cloud activity is stronger in parts of the tropics (Central Africa, West Pacific). This is surprising, because the CRISTA cloud detection method is less sensitive than the SAGE method following the argumentation of section 4.1. But the cloud activity during the CRISTA-1 period is not really representative of a climatology mean, and the discrepancy could be affected by the different data periods respectively due to variability in the cloud activity on timescales of days or weeks (see also section 4.4). The latter could be caused by phenomena such as Kelvin Waves for example or variations in the Madden–Julian oscillation.

[20] The CRISTA-2 to SAGE comparison is also in very good agreement at the 17.5 and 15.5 km level. The occurrences are lower for CRISTA-2, which is not surprising following the discussion in section 4.1. At the 13.5 km level (Figures 6c and 6f) larger differences can be observed, but

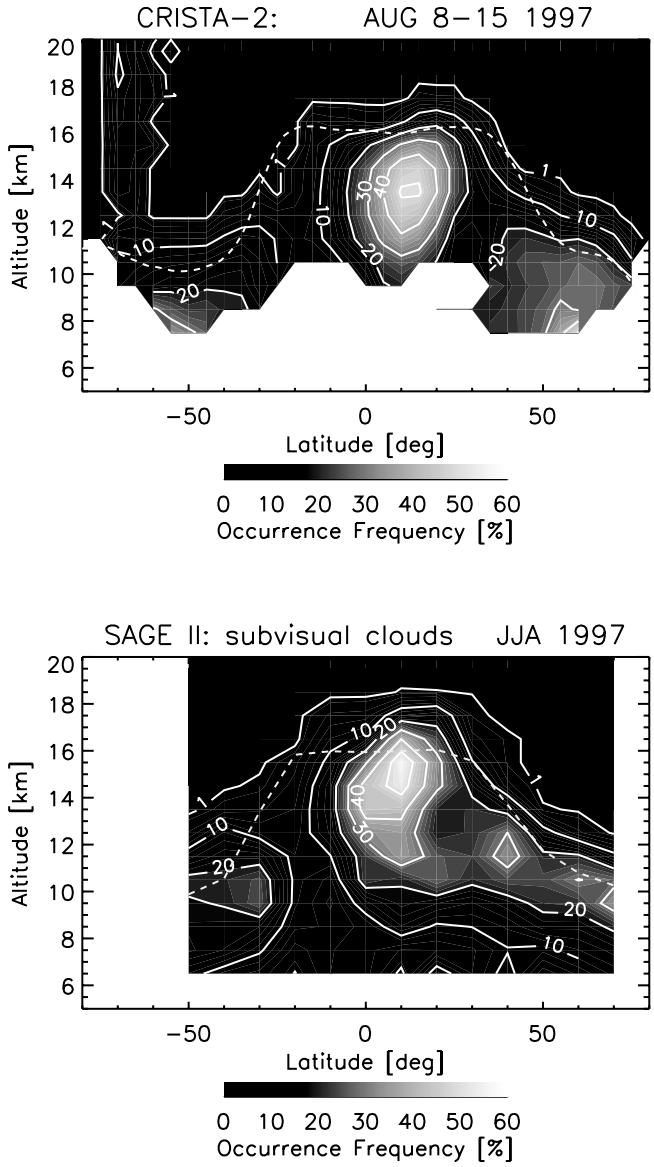

Figure 4. Zonal mean of cloud occurrence frequencies for (a) CRISTA-2 and (b) SAGE II June–August mean (JJA) for 1997 of SVCs (see text).

the horizontal spread of cloud occurrences into the midlatitudes is obviously the same for both statistics. Belts of high occurrence frequencies in the tropics have been observed for both missions but not at the same altitude (CRISTA-1 at 17.5 km and CRISTA-2 at 15.5 km). The statistics at 17.5 km look quite different for the two CRISTA missions. In general one finds much lower frequencies for the northern hemisphere summer conditions (CRISTA-2) than during the November flight, and only a single cloud activity center over the summer monsoon area (mentioned above) for CRISTA-2. This seasonal variability in the cloud activity at different altitude layers is predicted by the SAGE climatology and is generally in good agreement with the CRISTA observations. The seasonal variability may be influenced by the meteorological conditions of the tropical tropopause (TP). It is well known that the tropical tropopause varies in height and temperature during the seasons [*Reid and Gage*, 1981], which has also implications for the amount of water that enters the lower stratosphere by a reduced freeze-out effect [e.g., *Mote et al.*, 1996]. The annual minimum for TP height in July and August is accompanied by the warmest tropopause temperatures, which implies higher saturation mixing ratios for water vapor and higher temperature thresholds for the formation of ice particles for this season. For November *Reid and Gage* [1981] found a significantly colder (∼3 K) tropical TP, located at higher altitudes (∼1 km). This corresponds with the observation of larger cloud occurrence frequencies at higher altitudes during the first mission.

[21] In spite of the different vertical and horizontal resolution as well as data periods of both instruments the surprisingly good general agreement between SAGE and CRISTA shows that the comparison is quite useful. Furthermore it suggests that CRISTA often detects subvisual cirrus in addition to thicker clouds.

4.3. El Niño Signatures

[22] As mentioned above, the longitudinal location of the CRISTA maxima of cloud occurrences are in good agree-

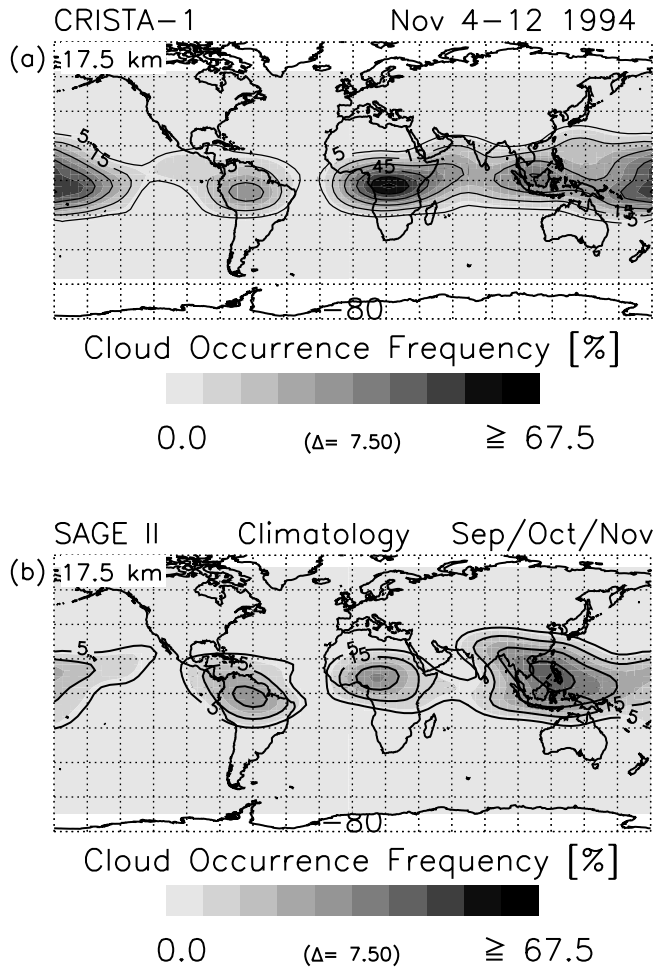

Figure 5. Latitude–longitude distributions of cloud occurrence frequencies between 17 and 18 km for CRISTA-1 (a) in comparison to the SAGE II climatology (b) of SVCs. Both statistics are based on a 24° × 10° × 1.0 km gridding. Contour lines of occurrence frequencies are plotted for 5, 15, 30, 45 and 60%.

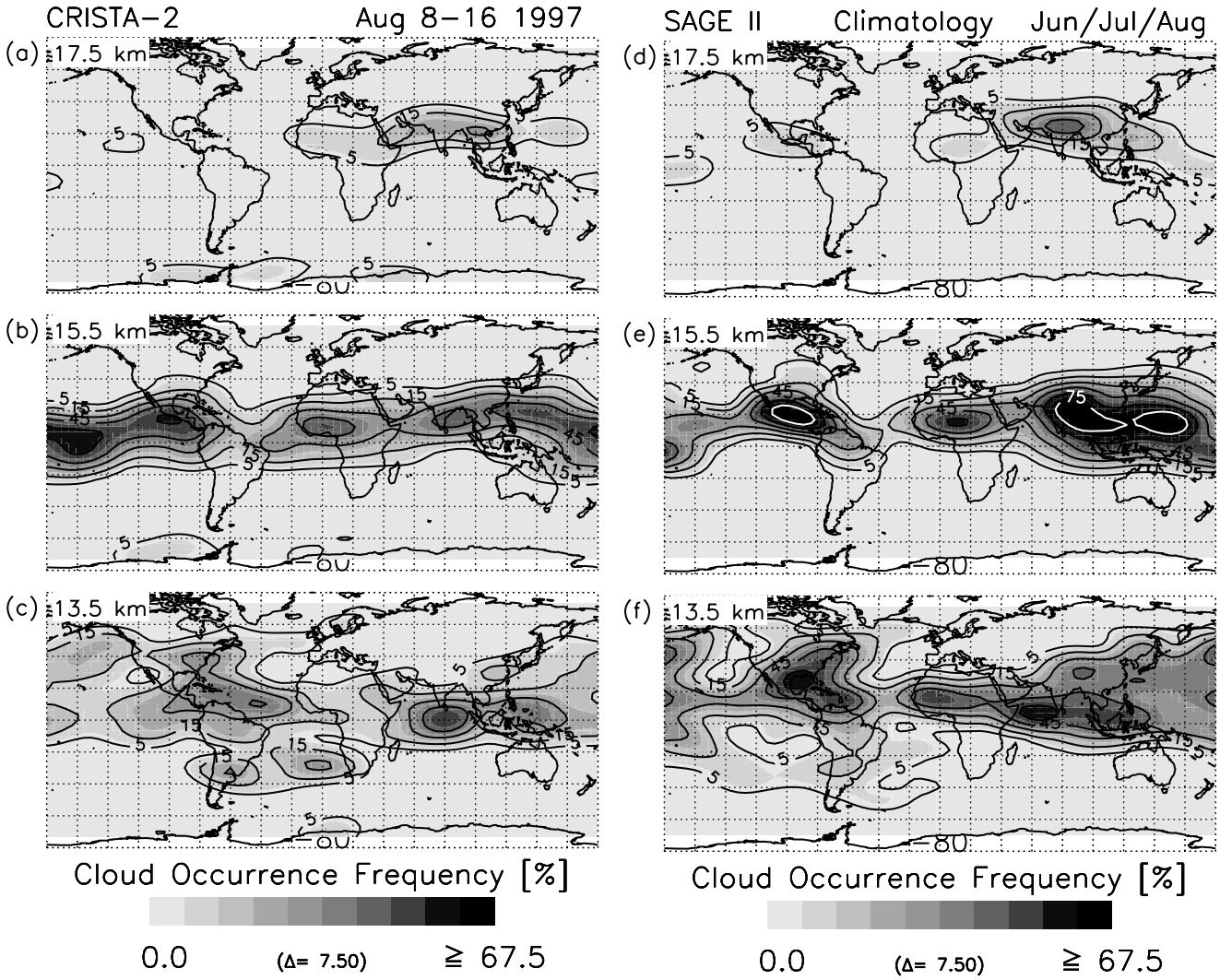

Figure 6. Latitude–longitude distributions of cloud occurrence frequencies at the altitude levels of 13.5, 15.5, and 17.5 km for CRISTA-1 (a–c) in comparison to the SAGE II climatology (d–f) of SVCs. Statistics are based on the same gridding as in Figure 5. Contour lines of occurrence frequencies are plotted for 5, 15, 30, 45, 60 (black), and 75% (white).

ment with the SAGE II climatology. However, the high cloud activity region observed by CRISTA-1 and CRISTA-2 around the date line (Figures 5a and 6b) is not detectable in the climatology and is presumably caused by El Niño events taking place during the two CRISTA periods. The tropical zonal circulation pattern (Walker circulation) changes completely during an El Niño event. The so-called warm pool and center of deep convection over the Indonesia/Micronesia region shifts in direction to the center of the Pacific, accompanied by a shift in the cloud activity over the date line. Enhanced cloud activity in the whole Pacific region during El Niño is easy to detect in Figure 7a, where differences between the CRISTA-2 and SAGE II SVC climatology have been calculated. Additionally in the Indonesia area a pronounced reduction in cloud activity is found. Also a slight reduction is observed over Central America.

[23] One way to relate the location of cirrus to the location of deep convective clouds in the tropics is to use the OLR as an indicator of deep convection [e.g., *Massie et al.*, 2000]. Deep convective clouds will radiate at cloud top at colder temperatures than clear-sky regions and also low-altitude clouds due to the tropospheric negative temperature gradient. Differences in the global distribution of OLR between El Niño and non-El Niño years will indicate anomalies in location of the preferred regions of deep convection. For Figure 7b Climate Diagnostic Laboratory OLR data [*Liebmann and Smith*, 1996] have been utilized. The data set has a longitude–latitude resolution of $2.5° \times 2.5°$. The differences between the mean OLR for August 1997 and mean for all August months for the SAGE period (1985–1990) show quite good agreement with the CRISTA/SAGE differences (Figure 7a). Enhanced OLR from the international date line to the coast of South America and reduced OLR above Indonesia and parts of the Indian Ocean seem to be connected with enhanced and reduced cloud activity respectively.

[24] The SAGE data set of 6 years for the climatology includes one El Niño period (1987). A significant increase in the tropospheric cloud occurrence (12.5 km) in the central Pacific was found for this period [*Wang et al.*, 1996], but the longitudinal variations in comparison to the

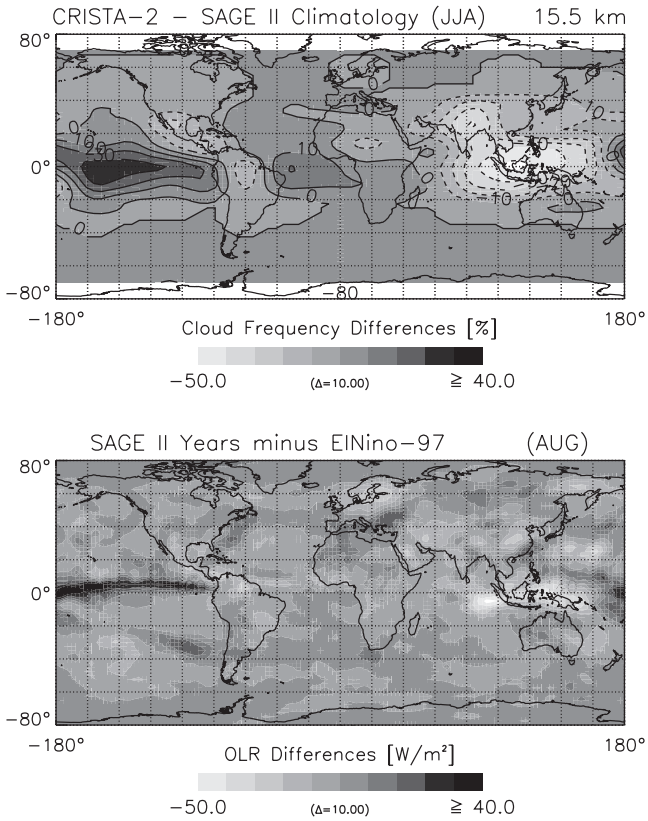

Figure 7. (a) Differences of cloud occurrence frequencies between the CRISTA CTH analysis and the SAGE II climatology for SVCs at the 15.5-km altitude level. The analysis is based on the same longitude–latitude height grid of 24° × 10° × 1 km. (b) OLR differences between the 1997 El Niño August mean and a 6-year mean of August mean values of the SAGE climatology period (1985–1990).

5 non-El Niño years have not been discussed above 13 km. More recent analyses by *Massie et al.* [2000] using extinction data of HALOE show evidence of increasing upper tropospheric cirrus (100 hPa) over the mid-Pacific and decreased cirrus over Indonesia for the 1997 El Niño conditions, which is in quite good agreement with the CRISTA-2 observations.

4.4. Daily Variability

[25] Up to now geostationary meteorological satellite have been unable to detect optically thin cirrus clouds around the tropopause. The variability in the cloud occurrences on scales smaller than a week are difficult to observe by nongeostationary remote sensing instruments. Due to the orbit and measurement geometry solar-occultation experiments like SAGE or HALOE need around four weeks for a complete latitudinal coverage. Therefore the resulting cloud statistics are useful for investigations of seasonal and interannual variability only. Limb-emission instruments need only one day for a complete coverage, but normally the sampling is too poor for significant statistics. To the authors knowledge, the CRISTA measurements are the first to make possible an estimation of the day-to-day variability of clouds around the tropical tropopause. The necessary large number of overpasses per day were achieved in the first CRISTA mission only, where the measurement sampling was very homogeneous and the latitude coverage was more restricted than for the second mission. The daily statistics of occurrence frequencies from 5 to 11 November (Days 309–315) at the 17.5 km level are presented in Figure 8. Data gaps are areas with observation numbers <10 in the specified grid box. The mean observation number per grid box is between 25 and 40 depending on the day, which reflects the statistical reliability of the data set. In the tropics and subtropics a roughly complete coverage was achieved for six days of the seven day period. The centers of highest cloud activity are fixed during the observation period at the localized regions of Figure 5a (Central America, Africa and the Pacific). But the activity of each center shows a very individual variation within one week. For example the large activity over Central Africa (>60%) on Day 309 decreases during the following days and starts to increase again at the end of the mission. The

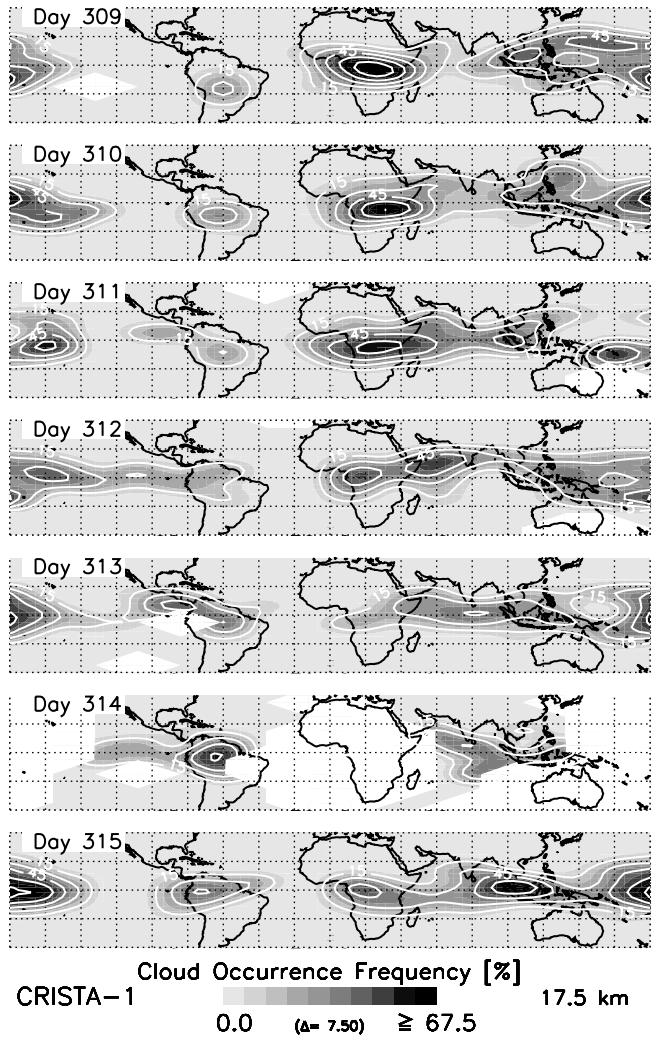

Figure 8. Daily cloud occurrence frequencies for the CRISTA-1 mission from Day 309 to 315 (5–11 November) in 1994. The statistics are based on the same gridding as Figure 5. Only the 40°S–40°N coverage is shown. Data gaps are areas with observation numbers smaller than 10 in the specified grid box.

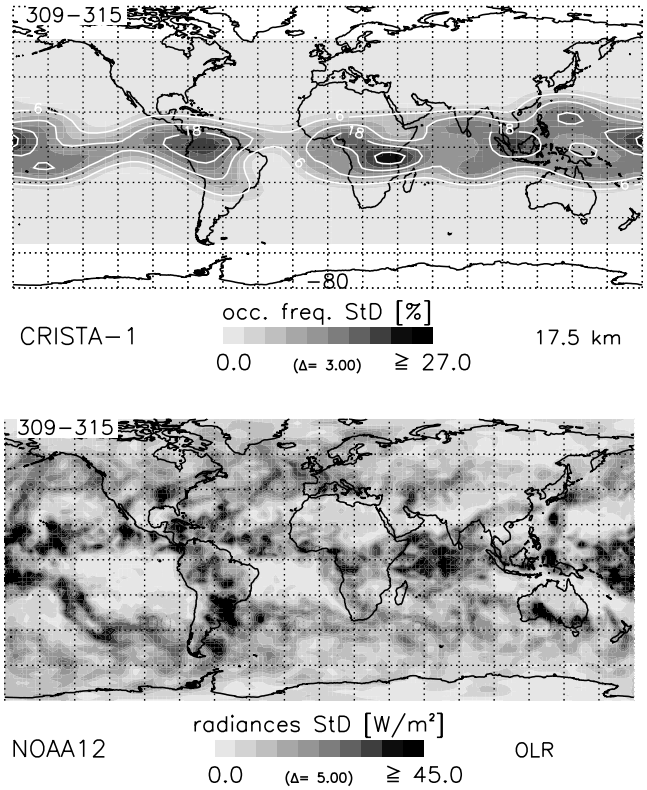

Figure 9. (a) Standard deviation of the 7-day observation period for CRISTA-1 cloud occurrence frequencies as shown in Figure 8. Only grid boxes with more than three observation days are taken into account. (b) OLR standard deviation of NOAA12 daytime measurements for the same period like CRISTA-1 in (a).

Indian Ocean together with the Indonesia area are characterized by high variability with no feature indicating an explicit center of activity.

[26] The standard deviation over the observed time period is a well known measure of the variability of a system. It is surprising to note that in Figure 9a the four pronounced regions of cloud activity show nearly the same maximum standard deviation (~20% absolute). However, centers and maximum standard deviation are not exactly in the same place (Figure 5a). Although the absolute value of the standard deviation is acceptable throughout the tropics, large areas with medium cloud activity (20–30%) show a variability of the order 30–50% of the observed occurrence frequency. This emphasizes the significance of variability in cloud activity on timescales of one week or several days.

[27] As mentioned above OLR is an indicator for deep convective activity and variability as well as induced waves and oscillations [e.g., *Salby and Hendon*, 1994]. Therefore the standard deviation in OLR can be used as a rough measure for the variability in deep convection (Figure 9b). Similarities between OLR and cloud occurrence frequencies are obvious, like the belt of high variability in the tropics which is slightly shifted to the northern hemisphere. However, only the mid-Pacific maxima is in good coincidence with the CRISTA observations. Other maxima/minima in the OLR are not detectable (e.g., maxima in OLR over the India ocean) or they are smeared in the occurrence frequencies by the coarse horizontal resolution. Convective activity and its variability are not necessarily coincident with the variability of cirrus clouds around the tropopause.

4.5. Uncertainties in Occurrence Frequencies

[28] High measurement densities result in significant statistics, which is generally the case for both CRISTA missions. The first mission had a mean observation number of 100–200 per latitude–longitude grid box, which implies that the CRISTA sampling density is good enough for statistics using a smaller horizontal gridding or daily based analyses (see results in section 4.4). Due to the extended latitudinal coverage the number of observations for the CRISTA-2 period are generally smaller with locally enhanced observation densities caused by special pointing modes of the instrument for validation measurements over Europe and North America as well as by the very high spatial resolution measurements over Indonesia [*Grossmann et al.*, 2002]. These special modes also produce reduced observations densities (<20) and a lower statistical significance in neighboring areas by regional data gaps during part of the mission.

[29] The presented cloud count statistics are equivalent to a binominal experiment. Therefore the two-standard-error bound for a grid box with a cloud occurrence frequency p can be specified by the simple formula [e.g., *Wackerly et al.*, 1996, p. 319]:

$$err = 2 \cdot \sqrt{\frac{p(1-p)}{N}} \cdot 100 \quad [\%]$$

with N the number of observations in the grid box. Figure 10 presents the so-called cloud statistical error at 17.5 km for CRISTA-1 and 15.5 km for CRISTA-2, the two main cloud occurrence levels. By this definition, *err* describes (with a probability of 95%) that the uncertainty for the cloud occurrence frequencies of Figure 5a and 6b will be less than the corresponding *err*-value. In general the occurrence frequencies are significantly larger than *err*, indicating that the results are statistically significant at the 95% confidence level. Obviously *err* is related to p and becomes significantly larger for occurrence frequencies around 50%.

[30] *Kent et al.* [1997] pointed out additional error sources for the detection of high altitude cirrus clouds by the limb geometry by simulations of SAGE II cloud measurements in conjunction with airborne lidar data. In transferring these to the CRISTA analysis they found out that the true altitude of a cloud may be higher than that found by the cloud detection method. This is caused primarily by clouds or cloud fragments within the line of sight, behind or in front of the tangent point layer. Errors of 1 km and more occurred in just under 40% of the simulations, but mainly at the lower cloud altitudes (10–12 km). Moreover, observations from space by the LITE experiment indicate that even in regions with deep convection, a so-called laminar cirrus (thickness <500 m) is often formed as a separate cloud layer 2–3 km above the convectively generated anvils with a mean horizontal extent of 500 km [*Winker and Trepte*, 1998]. To provide evidence for such extremely optically thin structures in the CRISTA data the cloud detection method used in the present analysis is not

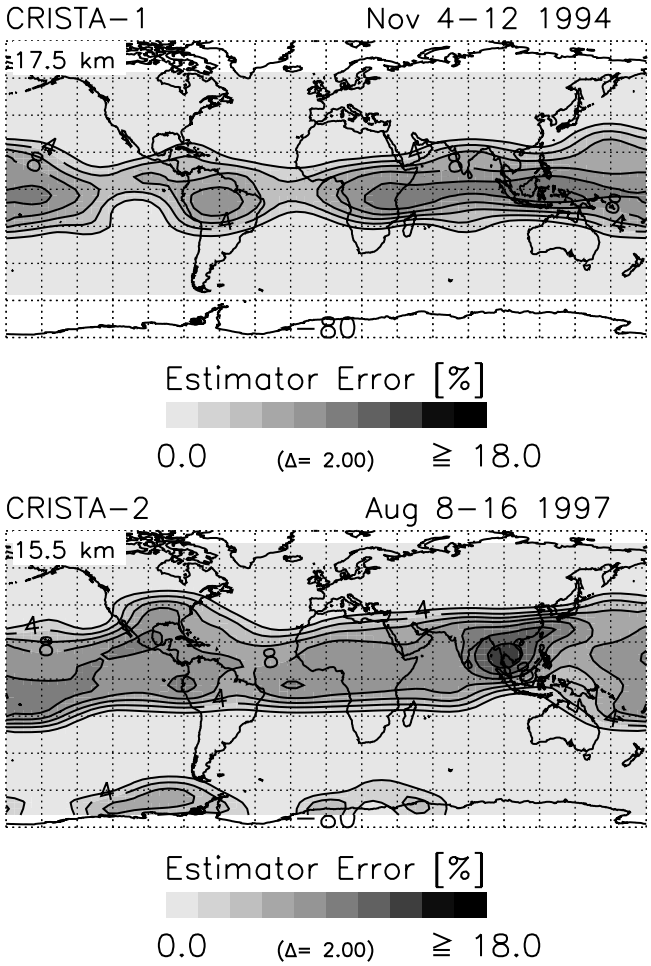

Figure 10. The two-standard-error bound for a cloud detection (probability) by the CRISTA-1 and CRISTA-2 occurrence statistics at 17.5 and 15.5 km, respectively.

sensitive enough and the vertical resolution of the instrument (1.5 km) is presumably too large as well.

5. Cloud Top Temperature

[31] As mentioned in section 4.2 the tropopause temperature and height might influence the formation and the occurrence of the cirrus clouds respectively. Cloud top temperature (CTT) and the vertical distance of the cloud top observation from the tropopause are also important parameters for the description of the cloud properties. Convectively generated cirrus clouds below the tropopause will be radiatively heated, but their temperature will still decrease as the cloud rises in an environment where the temperature decreases with altitude [*Ackerman et al.*, 1988; *Pfister et al.*, 2001]. The outflow ice crystals will continue to grow and large particles can fall out. Consequently the clouds advect moisture upward and remove it by sedimentation [*Sherwood*, 1999]. Above the tropopause radiative heating will cause the leftover ice crystals to evaporate and moisten the lower stratosphere.

[32] Figure 11 shows CTT in relation to CTH for one specific day of each mission (latitude range: ±40°). CTTs were taken from the assimilated temperature fields of the Goddard Space Flight Center (GSFC) Data Assimilation Office (DAO) [*Schubert et al.*, 1993]. A negative correlation between CTT and CTH is found. The distribution follows the typical tropospheric temperature gradient (lapse rate) and is also partly caused by the latitudinal dependence of the tropopause (TP) temperature (decreasing TP height and increasing TP temperature with increasing latitude). Obviously the two missions show a different behavior. During CRISTA-1 significantly more clouds were observed above the tropical and subtropical tropopause than for CRISTA-2 (42%/25% for cloud observations above 15 km, complete mission). For both missions the mean distance between TP and CTH is very similar (0.5 km/0.7 km). But

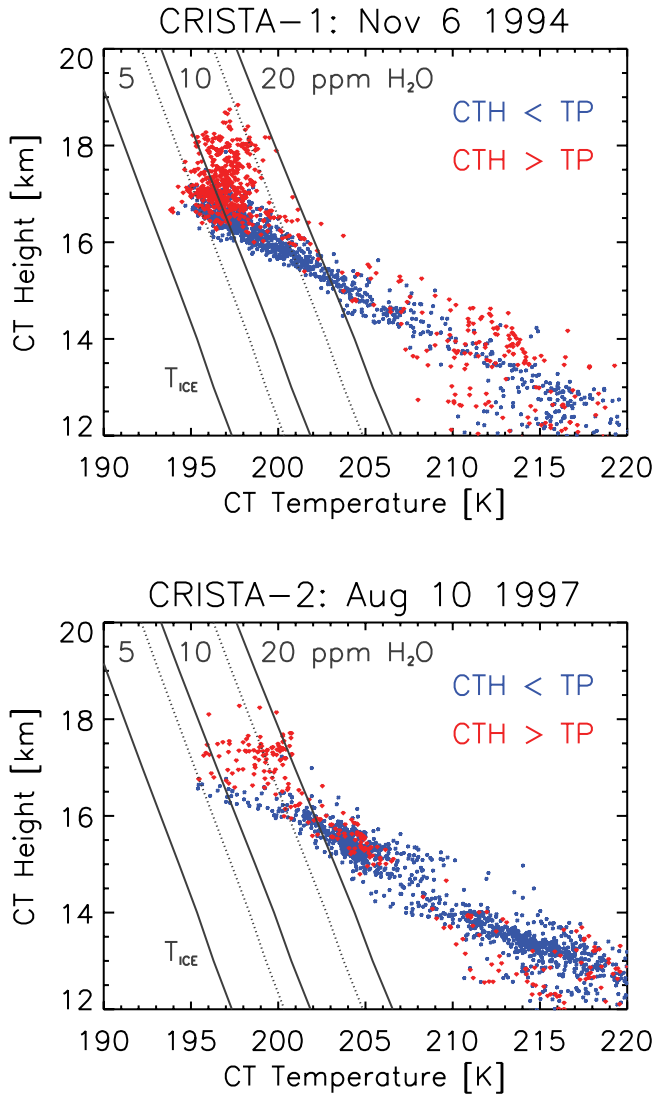

Figure 11. Scatterplot of cloud top temperature versus CTH for two single days of either CRISTA mission, (a) 6 November 1994 and (b) 10 August 1997 for latitude range ±50°. The colored symbols indicate CTHs above (red) and below (blue) the thermal tropopause, respectively, defined by the WMO criterion of 2 K km^{-1} gradient above 500 mbar. Ice condensation curves for 5, 10, and 20 ppmv water vapor are given as thin gray lines (after the work of *Marti and Mauersberger* [1993], without supersaturation and aerosol) as well +3 K shifted curves for 5 and 10 ppmv.

the CRISTA-1 events above the TP reach higher mean altitudes (17.3 km/16.6 km) and also colder temperatures (197 K/201 K). A very similar behavior was observed for the CTH below the tropical TP. The results are in line with the mean tendency of a colder and higher tropical tropopause during November compared with August conditions [*Reid and Gage*, 1981, 1996]. Ice nucleation at lower temperatures should generate larger ice crystal densities, resulting in slower sedimentation speeds and longer cloud lifetimes [*Jensen et al.*, 1994, 1996b]. Estimated cloud lifetimes for CRISTA-1 and CRISTA-2 using OLR fields in conjunction with trajectory analyses look equal and cannot support the latter fact (for details, see section 6.4 and Figure 16). However, the large occurrence frequencies during CRISTA-1 at the 17.5 km altitude level (Figure 5) could be affected by a longer cloud lifetime, which implies a larger probability of observation.

[33] The ice saturation curves in Figure 11 imply that the CT temperatures are too warm for ice condensation assuming typical water vapor mixing ratios around the tropical tropopause (<5 ppmv). Consequently the observed clouds are presumably not generated under the synoptic conditions described by the analyzed meteorological fields. Although, the analyzed temperature around the tropical tropopause includes, in general, warm biases of 2–4 K in comparison to radiosonde measurements (3 K for DAO temperatures at 100 hPa [*Pawson and Fiorino*, 1999]). This is quite a remarkable effect and is equivalent to a shift in the saturation curves (dotted lines). In this case potentially ''drier'' conditions are conceivable for the formation of the observed clouds.

[34] Microphysical model studies by *Jensen et al.* [1996b] have shown that thin cirrus clouds in the upper troposphere and lower stratosphere can be formed by buoyancy waves or slow vertical motions, if aerosol particles are present. The sulfate aerosols will take up water and spontaneous freezing can occur. Consequent sedimentation of ice particles can dehydrate the tropopause region, most effective for the slow cooling mechanism. Therefore, an entrainment of ''wet'' and ice-saturated air masses by deep convection is not essential for the formation of the observed clouds above 16 km. However, modeled cirrus clouds by *Jensen et al.* [1996b] were generated at significantly colder temperatures (~187 K) than the observed CTTs (T_{min} ~ 195–197 K).

[35] Almost all clouds above the tropopause for CTT >205 K and CTH <15 km are observations from midlatitudes. The limited CRISTA-1 measurements at altitudes below 15 km did not permit global statistical analyses in the midlatitude tropopause region (section 4.1). However, a significant number of cloud events above the tropopause could be verified for both missions. This is quite important, because midlatitude ozone trends are largest exactly in this altitude region and could be partly caused by heterogeneous chemistry on cirrus particles [*Solomon et al.*, 1997].

6. Trajectory Analyses

[36] Cirrus clouds are normally expected to be observed above areas of deep convection. However, cirrus clouds around the tropical tropopause have also been detected in regions obviously not associated with deep convective systems [e.g., *Pfister et al.*, 2001]. Microphysical model studies have shown that thin cirrus clouds may persist in the cold western Pacific tropopause region for days, before they are advected out of the region and heated by subsidence [*Jensen et al.*, 1996a].

6.1. Location of Deep Convection by OLR

[37] To set the CRISTA observations of clouds around the tropical tropopause in relation to deep convection centers, OLR data of the NOAA12 satellite have been used as a proxy for deep convection. The OLR data set has a horizontal resolution of 2.5° × 2.5° and is processed on a daily basis [*Liebmann and Smith*, 1996]. The Sun-synchronous polar orbit of the NOAA12 satellites allows additionally one day (descending node: ~0730 local time [LT]) and one night measurement (ascending node: ~1930 LT) for each location. This is a similar time pattern as the CRISTA tropical observations with 12 hours shifted local time for ascending and descending node measurements. However, the equator crossing times shifted during the mission by around −2.5 hours (ascending node start of mission: ~0700, descending node: ~1900).

[38] Figure 12 shows two exemplary OLR maps for the CRISTA-1 and CRISTA-2 period in comparison to the CRISTA high altitude cirrus cloud observations. Deep convection is indicated by OLR values smaller than 200 W m^{-2} [*Weaver et al.*, 1998] and in the following this threshold is used as a rough indicator of deep convection (Figure 12, dark green to violet). Indeed, there is some correspondence between OLR and high cloud observations in the tropics. The northern shift in deep convection activity in the OLR for the northern summer conditions of the second mission is nicely reproduced by the CRISTA cloud detection. However, there are also areas of significant disagreement in Figure 12. A count statistics for both mission shows that less than 25% of the cloud observations are temporally coincident with deep convection centers. Since the exact optical depth of the clouds is unknown, it is difficult to judge how remarkable their occurrence far from convection is. There are three possible reasons for the surprisingly low correspondence between OLR and the cloud observations by CRISTA. (1) The 12-hourly temporal resolution for the OLR maps is not good enough for a quantitative comparison. Convective systems are present on timescales of hours and deep convection may be at a different location between the OLR and CRISTA sampling time. (2) Due to transport processes by partly strong horizontal winds (e.g., up to 10–20 m s^{-1} at 380 K) the cloud observations are not necessarily fixed relating to the centers of deep convection [*Jensen et al.*, 1996a]. (3) Some of the clouds observed are formed in situ by cooling events on a synoptic or gravity-wave scale and are not triggered by deep convection systems. Trajectory mapping of the cloud top location using assimilated winds in the upper troposphere and lower stratosphere is a reasonable way to establish the consistency of the convective history of the observed clouds around the tropical tropopause [*Pfister et al.*, 2001].

6.2. Trajectory Technique

[39] The trajectory model used in this study is described by *Bacmeister et al.* [1999]. In the analysis each starting parcel represents an individual cloud location observed by

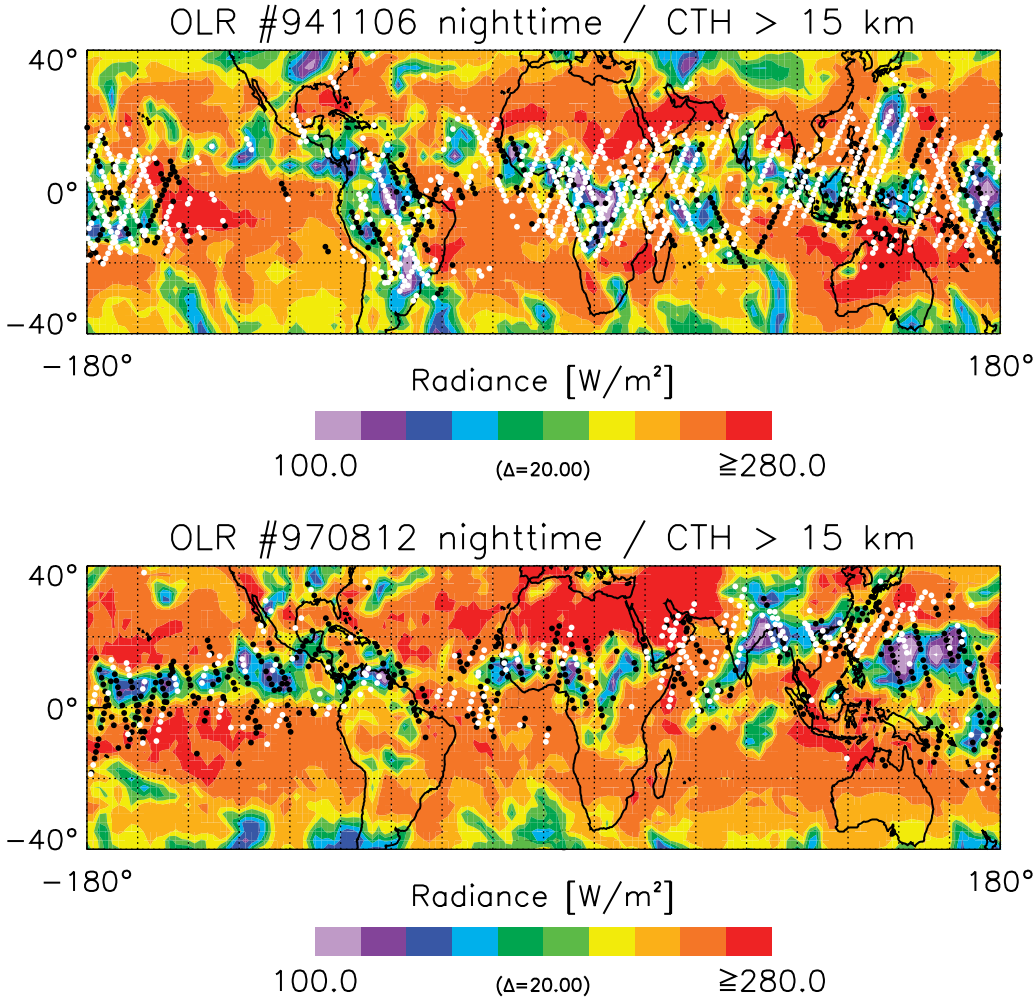

Figure 12. Comparison of NOAA12 OLR nighttime measurements and CRISTA-derived geographical locations of cloud tops for 6 November 1994 (CRISTA-1) and 10 August 1997 (CRISTA-2) in the 40°S to 40 °N latitude band. For CRISTA-1, white dots indicate cloud tops above 380 K isentrope and black dots below it. A 375 K isentrope is used for CRISTA-2. Only CTHs above 15 km are taken into account.

CRISTA. The calculations are adiabatic, that is, all parcels are assumed to remain on their initial isentropic surface. The meteorological data are obtained from the GSFC DAO. They are available at 6-hour intervals on a 2.5 × 2.0 longitude–latitude grid [*Schubert et al.*, 1993]. A conservative 5-day limit for backward calculations is chosen, due to the limitations on the length of time over which a trajectory calculation is valid because of uncertainties of the wind fields and diabatic effects. For statistical analyses the trajectory data are stored with a resolution of one hour only.

[40] Figure 13 gives an example of how the trajectory study works for the western Pacific and Indian ocean region. The OLR shows strong indications of deep convection from the eastern part of India to Indochina and the southern part of China, which is typical of the summer monsoon, and an additional large center north of New Guinea. In the latter region a tropical typhoon called Winnie was present, drifting slowly in direction to the southeast of China during the mission. Standard meteorological weather analyses show that the largest activity of the typhoon occurred on 12–13 August (Class 5). Most of the observed cirrus cloud (>15 km) are not coincident with deep convection centers in the OLR. The backward trajectories are only superimposed if the 5-day backward trajectory has crossed an OLR defined deep convection area (OLR < 200 W m^{-2}). The individual trajectory starts at the date of observation and ends at the time step when the parcel enters a deep convection area. The OLR value for each time step was calculated by spatial interpolation (surrounding four OLR grid points). Furthermore we have made the rough approximation that the deep convection activity in OLR snapshots (only two local times) are representative for a ±6 hour period in relation to the OLR observation time.

[41] The cirrus clouds above southern Saudi Arabia and the Arabian sea are regions without deep convection activity in the OLR (>240 W m^{-2}) during the complete mission. The backward trajectories show very well that the origin of these high altitude cirrus clouds is found in the monsoon induced deep convection areas above the Indian Ocean and Indian continent. Large numbers of cirrus clouds are also observed right in between the southeast coast of China and typhoon Winnie, which is nicely documented by the high sampling rate of a special CRISTA measurement mode.

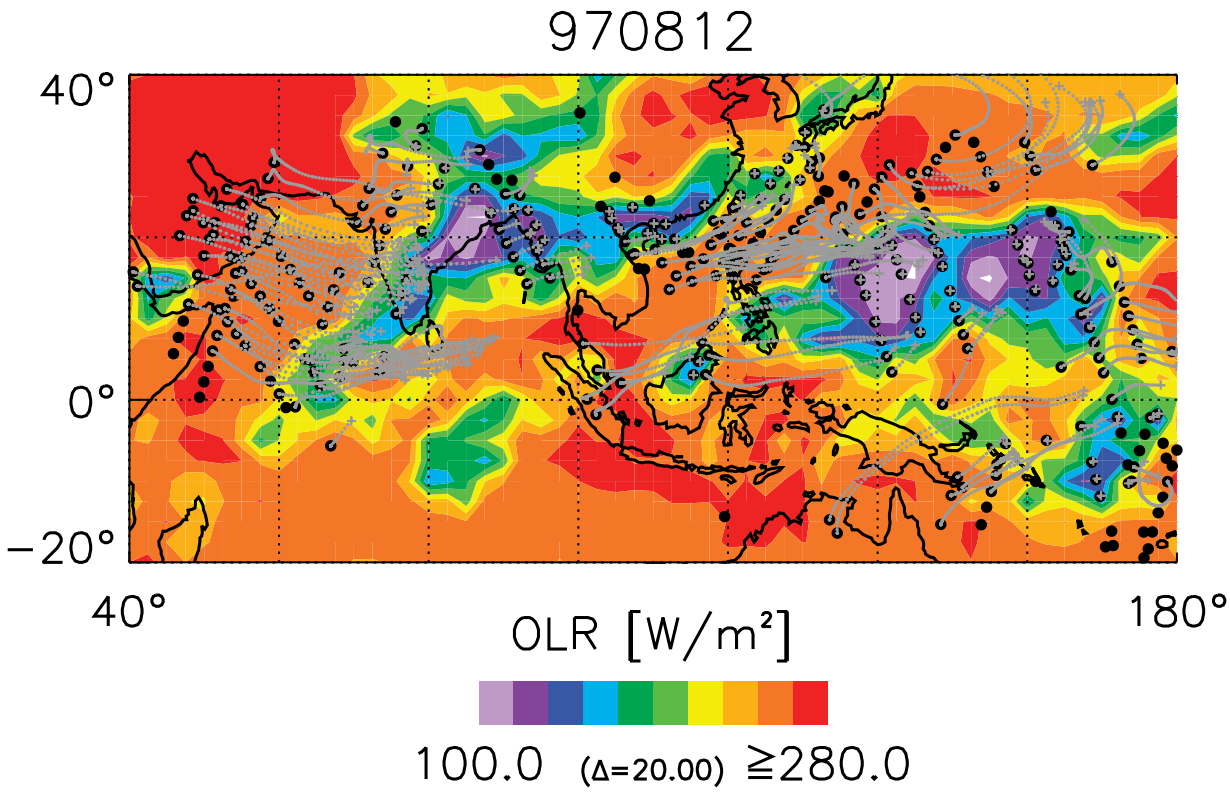

Figure 13. OLR distribution and CRISTA cloud observations above 15 km in conjunction with backward trajectories in the longitude range 40°–180°E. The trajectory resolution is 1 hour (see text).

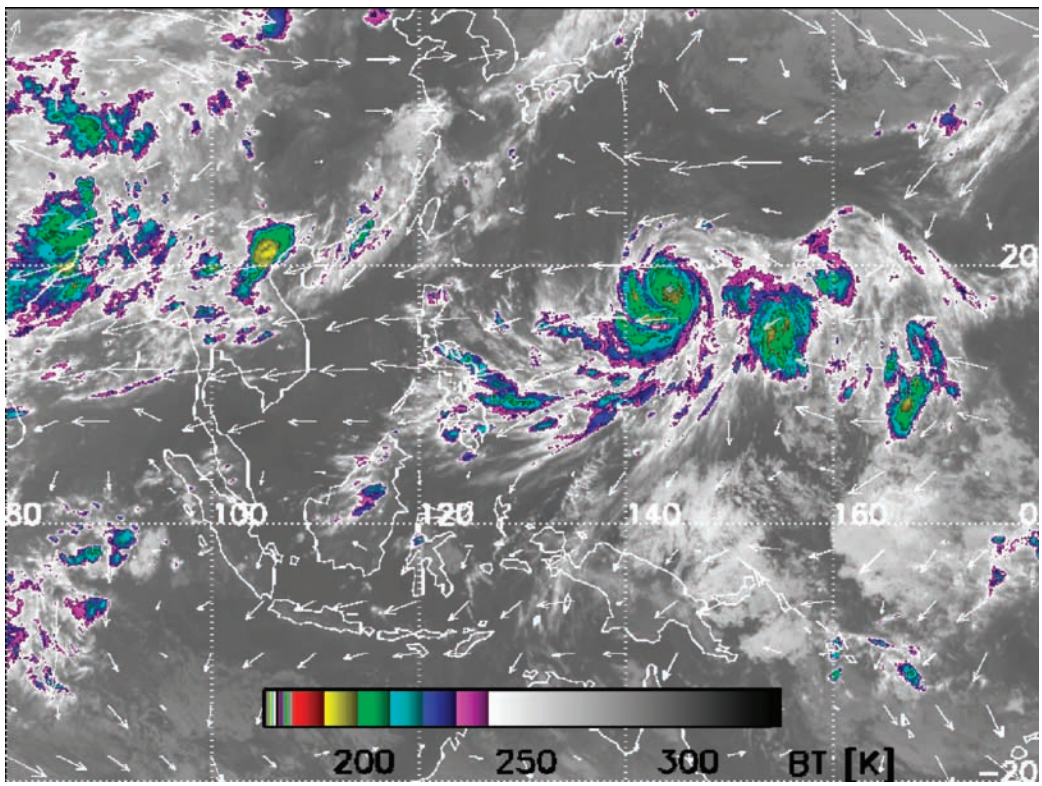

Figure 14. BT at 10.5 μm as observed by GMS and GOES-9 meteorological satellites on 12 August at 1200. The latitude coverage is restricted from −20° to +40° and in longitude from 80° to 180°E. The color code indicates the tendency to high BT by white to gray (indication of lower tropospheric clouds and Earth's surface) and low BT by magenta to red (indication of high-reaching upper tropospheric clouds). Average winds of the DAO are superimposed for the 380 K isentrope level.

During this so-called Hawk-Eye mode the ASTRO-SPAS carrier was pointed at the same location on three subsequent orbits, in this case the Indonesia area, which results in an extremely high horizontal resolution of around 100 km $\times$100 km [*Grossmann*, 2000]. As in the previous example most of the observed cirrus clouds could be explained by the convective history. This is indicated by backward trajectories matching the typhoon area or a deep convection area southeast of Korea. The latter region is detectable in the OLR maps of the previous days.

6.3. GOES/GMS Statistics

[42] In a case study for the CRISTA-2 period, infrared satellite pictures of the geostationary meteorological satellites GMS-5, GOES-10 and GOES-8 have been added to the analysis for a more detailed view of the cirrus cloud observations downstream of deep convection areas. The great advantage of this data set is the 3-hourly time resolution, which is better than the OLR data (12 hours), and the high horizontal resolution of 0.1° $\times$ 0.1°, which allows the detection of small localized deep convection anvils. These small potentially sources or cirrus clouds are not well represented in the OLR data set. The combined longitudinal coverage for the three satellites is restricted from 80°E to 60°W (equivalent to 72% coverage of the tropics and midlatitudes). Figure 14 shows the brightness temperature (BT) of the GMS 10.5 μm channel for 12 August at 1200 in the west Pacific region. Typhoon Winnie is easily detected as spirals of cold and high reaching clouds. Similarities with the OLR distribution of Figure 13 are obvious, just as in the cloudy Indochina region. Anyway, the BT is much more structured than the OLR and the temporal variability is large (diurnal variation, not shown). The superimposed wind vectors at the 380 K isentrope show strong easterly winds starting from the west side of the typhoon region.

[43] For the trajectory statistics concerning the BT fields we followed the analysis technique of *Pfister et al.* [2001]. In a first step one can assume that a backward trajectory has reached a convective cloud if the BT is less than or equal to the parcel temperature. This is only correct for the optical thick core of the convective system, where differences between cloud top temperature and BT are small. In the optical thinner outer part of the anvils differences become significant [*Liou et al.*, 1990] due to the translucent warmer background of the Earth's surface or warmer clouds at lower altitudes. We use the same simple approach to correct this effect as Pfister et al. The size of a localized convective system is on the order of 1° $\times$ 1° and the CTH of a tropical anvil is roughly constant [*Danielsen*, 1993]. Therefore we assumed that the BT at any position in a typical 1° $\times$ 1° square is actually equal to the minimum BT in that square, provided that there is a significant cloud at that position. Pfister et al. defined a significant cloud at BT <240 K, equivalent to an optically thick cloud with an altitude of about 9 km, the lowest level for which significant detrainment occurs in large mesoscale tropical convective systems [*Houze*, 1989]. The method described above results in a more flattening BT distribution. The computed BT maps represents a more realistic picture of the actual cloud top temperature than the BTs themselves and were used for the following trajectory analysis.

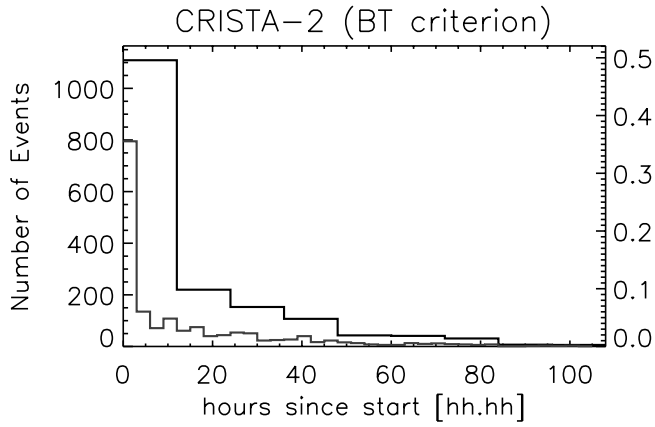

Figure 15. Count statistics of backward trajectories, which have reached a deep convection area defined by the BT criterion (for details, see text) within a 5-day period for each individual CRISTA CTH observation above 15-km altitude. The right vertical axis indicates the counts in relation to the total number of processed trajectories (2237). The longitude area was restricted from 80°E to 60°W due to the combined GOES/GMS coverage. The gray line indicates the statistics in 3-hour bins, the temporal resolution of BT fields. For the black line, 12-hour bins are used for better comparisons with the OLR statistics.

[44] In addition, Pfister et al. argued that rapid anvil heating during a short period in which the anvil is optically thick can lift the anvil to higher altitudes. In this way convective clouds that initially reach lower altitudes and warmer temperatures than the parcels along the back trajectory can actually reach those trajectory parcels and inject air and ice particles into them. The radiatively forced ascent implies a temperature decrease on the order of 3–10 K for typical temperature lapse rates at the tropical upper troposphere [*Pfister et al.*, 2001]. Therefore we have defined convective interaction along the trajectory as BT is less than 10 K warmer than the parcel temperature. This should represent the largest amount of convective influence along a trajectory.

[45] The resulting count statistics in Figure 15 show that a very large part (78%) of the calculated total number of 2237 trajectories are connected to deep convection centers. The statistics decay rapidly at short distance/trajectory length (t_{traj} < 12 h), for example the first 3 hours includes 35% of the events. However, for longer periods the decay is at a slower approximately linear rate. For t_{traj} > 12 h 28% of the total number of 2237 trajectories have reached a deep convection. No significant number of trajectories were found for t_{traj} > 86 h. Therefore, the maximum life time of the observed cloud t_{max} can be cautiously estimated at 3–4 days.

6.4. OLR Statistics

[46] As the GOES/GMS data set was available only for the CRISTA-2 period and restricted in longitude range, the OLR data set was used for a comparison between both missions and seasons respectively. For the detection of trajectories linked to deep convection the simple approach described in section 6.2 was used. The limited temporal and spatial resolution of the OLR allows only qualitative studies

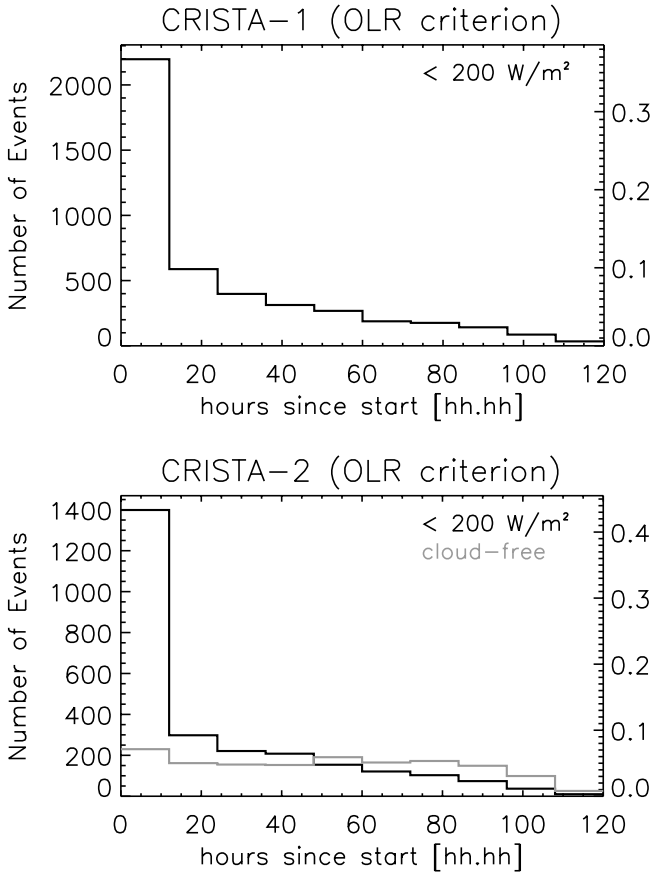

Figure 16. Count statistics for both CRISTA missions of backward trajectories reaching a deep convection area defined OLR < 200 W m^{-2}. The right vertical axis indicates the counts in relation to the total number of processed trajectories and observed CTHs (5983/3228 for CRISTA-1/2), respectively. For CRISTA-2, a trajectory count statistic at 380 K for all noncloudy profiles (7476) is superimposed (gray graph). The total number fraction is given (right vertical axis).

on 12-hourly binned statistics. Both statistic (Figure 16) show a very similar behavior also in comparison to the BT analysis, but the percentages are slightly different. The cumulative percentages of 73% and 81% of the trajectories for CRISTA-1 and CRISTA-2 are linked to an OLR-defined deep convection area. The difference between the two missions could be affected by seasonal variability in deep convection activity and the maximum height of the observed clouds respectively. For t_{traj} > 12 h 37% for CRISTA-1 and 40% for CRISTA-2 were found, which is larger than in the BT analysis. In addition, for both missions the gradient of the distribution is nearly identical in spite of different seasons when the observations took place. Statistics for t_{traj} up to 10 days yield no significant additional number of events greater than 4.5–5 days. A cautious estimate of a maximum lifetime of the clouds would give 4–5 days.

[47] Differences between OLR and BT analysis cloud be caused by the different techniques of the analyses and different horizontal resolution of the data sets. However, the results are very similar on a qualitative basis, which implies no obvious seasonal differences between August and November and the estimated maximum cloud lifetimes of around 4 days for deep convective induced cirrus clouds above 15 km altitude appears to be plausible.

6.5. Discussion of the Trajectory Results

[48] The assumption that the cirrus clouds persist along the trajectory down to the observation point is not necessarily correct. *Pfister et al.* [2001] have shown that any residual ice crystals from convective outflow will almost certainly evaporate due to stronger warming events (2–3 K) along the trajectory prior the parcels arriving in the area of observations. They have also determined, that the combination of convective influence and temperature histories is a very good predictor of whether a cloud would be found or not. We have checked the "evaporation effect" for the CRISTA data set by analyzing the maximum temperature increase in relation to the parcel temperature at the location of the deep convection impact. Only less than 1% of the considered trajectories in Figure 15 show warming events larger than 10 K, only 3% greater than 5 K, and 7% warmer than 3 K. Therefore evaporation effects might only slightly bias the trajectory statistics. The used trajectory method cannot prove that the clouds were cirrus blow-off or not, but in conjunction with the verification of evaporation effects it seems to be the best predictor of convective influence on the observed clouds.

[49] In addition we have tested the significance of the estimated cloud lifetime by two different methods. First trajectories for randomly chosen locations of CTHs were computed and statistically analyzed. The random statistics showed that the analysis method becomes insignificant for trajectory lengths greater than 3 days (no significant difference between random and CRISTA statistics). This implies that any estimate of cirrus lifetimes above this threshold becomes uncertain. A better test might be to utilize the method for all noncloudy profiles (negative test). The backward trajectories on an isentrope of 380 K for all noncloudy CRISTA-2 profiles have been analyzed for the BT and OLR data set (5105 and 7476 respectively). In general a constant behavior in percentages was found, which means that air parcels starting at a cloud-free area will reach a deep convection area after 12, 24 . . . 84 hours with a constant rate of probability (Figure 16b). This is quite different to the observed cloud trajectories with a decrease in percentages for increasing t_{traj}. In addition, it shows that the decrease has a physical reason and is not a statistical artifact of the method. Nevertheless the significance of the trajectory method is limited on t_{traj} < 3–4 days and cirrus lifetimes of up to 4 days appear to be realistic. Uncertainties in the trajectories (horizontal winds and temperatures) can also bias the presented statistics and this was minimized by the relatively short trajectory calculation (<5 days). Also the coarse 280 km length of the CRISTA sample volume is an additionally error source.

[50] The cloud lifetime estimated by the CRISTA results is generally in good agreement with the analyses by *Pfister et al.* [2001] mentioned above (trajectory lengths of 0.5–3 days since the most recent convection). The analysis was restricted to a relatively small corridor in the west Pacific only and is now supported on a more global basis by the CRISTA cloud observations. The large lifetime for the

observed cirrus clouds suggests that convective outflow cirrus are not dissipated rapidly, but can remain in the tropopause region for extended periods of time. This could be an important finding, since it increases the potential of cirrus clouds for influencing the radiation budget [*Jensen et al.*, 1996a]. This effect is difficult to quantify by the CRISTA data, because the optical thickness of the observed clouds is not as yet exactly to determine (see also section 3). A long lifetime of the cloud could also affect the chemical efficiency by heterogeneous reaction on the surface of the ice particles.

[51] By the simplifying assumption that clouds without convective history will be in situ formed, it is possible to estimate the amount of nonconvectively generated cirrus clouds to be 20–30%. However, the distinction between in situ formed and convective outflow cirrus is not really straightforward. The slow vertical motion for the cirrus formation mechanism described by *Jensen et al.* [1996b] may be driven by flow over convective systems. In this case, an induced cirrus cloud would be difficult to distinguish from a deep convection induced cloud, especially in the OLR analysis.

[52] Wave motions over longer periods (e.g., Kelvin waves) and convectively generated gravity waves (GW) may also generate sufficiently cold temperatures at the tropopause for the formation of cirrus clouds [*Pfister et al.*, 2001; *Jensen et al.*, 1996b]. Both types of waves have been detected in the retrieved CRISTA temperatures during the missions [*Smith et al.*, 2002; *Preusse et al.*, 2001]. For example the induced temperature disturbances by Kelvin waves during the first mission slightly above the tropical tropopause are in the maximum order of 2–3 K [*Smith et al.*, 2002]. This produces a quite remarkable effect on the water vapor saturation mixing ratio (e.g., 4.5 ppmv to 3.2 ppmv from 192 to 190 K at 100 hPa). In Figure 11a the temperatures are based on synoptic meteorological analyses without indications of Kelvin wave signatures. The reduction in CT temperatures by the observed Kelvin waves in conjunction with the DAO warm bias around the tropical tropopause (section 5) would be now sufficient for the formation of a small part of the observed cirrus clouds (coldest, CTT < 196 K in Figure 11a).

[53] First global distributions of convectively generated GWs are reported by *McLandress et al.* [2000]. GW excitation of the middle stratosphere processed by the Microwave Limb Sounder (MLS) radiance data revealed a spatial correlation with the OLR as a proxy for deep convection. A similar result is shown in Figure 17 for the CRISTA GW analyses [*Preusse et al.*, 2001]. The mean of significant large GW amplitudes (>3 K) at 25 km and 20°N (Figure 17b) shows behavior very similar to the OLR (Figure 17c) along the latitude circle. The additionally close correspondence with the presented upper tropospheric water vapor by MLS (Version 5.0) (W. G. Read et al., UARS MLS upper tropospheric humidity measurement: Method and validation, in preparation, 2001), also a proxy for regions of deep convection, may lead to the conclusion that the observed GWs are generated by convective systems.

[54] Since CRISTA GW analyses are currently only available above 20 km, it is very difficult to conclude that the observed GWs have also the potential to form ice clouds in the tropopause region, even though it is quite possible. Furthermore, the count numbers for the large GWs are notably smaller than the cloud count numbers at 16 km (not shown). This suggests that only a slight increase in the cloud occurrence frequencies due to GW (Figure 17a) may be expected. The only moderate correlation of the occurrence frequencies in relation to the GW, OLR and water vapor observations supports this assumption and from the analyses presented earlier it follows that convectively generated GWs certainly cannot be the only cause of the thin cirrus clouds observed by CRISTA. In addition, this circumstance emphasizes the relevance of the investigations of the convective history of high altitude cirrus based on trajectory calculations.

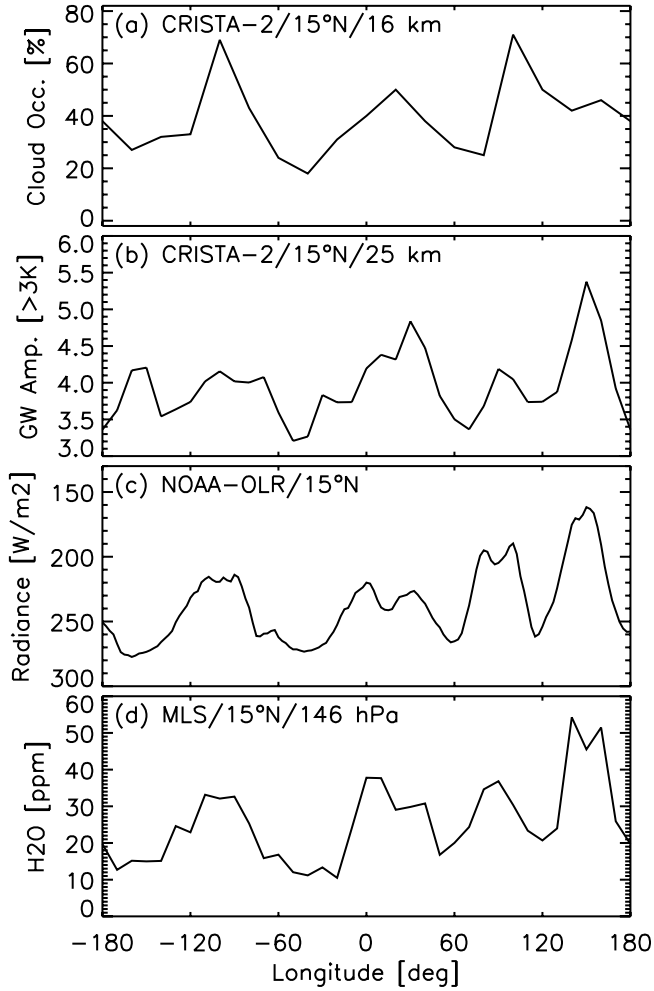

Figure 17. Intercomparison of the longitudinal distribution at 15°N (±5°) of (a) CRISTA-2 cloud occurrence frequencies at 16-km altitude level, (b) mean gravity wave amplitude at 25-km altitude for amplitudes greater than 3 K, (c) mean OLR (please note the reversed OLR range), and (d) mean upper tropospheric water vapor of MLS (Version 5.0) at 146 hPa. All mean values are based on the time period of the second CRISTA mission (8–15 August 1997).

7. Summary and Conclusions

[55] A simple but effective CI for thin cirrus clouds around the tropopause adapted from the measured IR spectra was developed and tested under different extreme atmospheric conditions. The deduced threshold is comparable with

extinctions of greater than 2×10^{-3} km^{-1} at 12 μm. CI and CTHs presented in this study are useful tools for the detection of polar stratospheric clouds and clouds around the tropopause. The tropical and midlatitudinal cloud occurrence frequencies are generally in good agreement with the SAGE II climatology and the 1997 analysis for SVC. However, discrepancies are observed in the Pacific region due to disturbances in the tropical circulation pattern caused by El Niño events. The latter was confirmed for the second mission by using OLR fields as a proxy for deep convection activity at different seasons and in different years. The dense measuring net during CRISTA-1 has enabled first analyses to be made of the daily variability in cloud occurrence frequencies around the tropical tropopause, which show significant day-to-day variability in various regions. Even though each mission was of short duration (one week) the large number of observations for both missions results in a high statistical significance for the occurrence frequencies. For both CRISTA missions a significant number of cloud events could be observed around the midlatitude tropopause. This is a relevant finding, because this region shows very large ozone trends in observations [*Solomon et al.*, 1997] and trends are reproducible by models if heterogeneous chemistry on cirrus particles is implemented.

[56] The present CRISTA cloud indication scheme does not allow a definitive distinction between optically thick and thin clouds (optical depth). More sophisticated analyses are necessary and could lead to a classification into subvisible and visible clouds respectively. The wide spectral range of the CRISTA measurements (4–15 μm) has the potential to determine microphysical parameters and to distinguish different cloud types by characteristic emission features.

[57] Extensive areas of high-reaching cirrus clouds (>15 km) have been observed in the CRISTA data downstream of deep convection systems. These cloudy regions are often (mostly) not detectable by the IR channels of geostationary satellites or in the OLR of NOAA12. Statistics of OLR and BT fields in conjunction with backward trajectories provide a consistent picture showing that 70–80% of the clouds around the tropical and subtropical tropopause are likely to have a convective history. Consequently at least 20–30% of the high cirrus may be in situ formed by cooling events on a synoptic or gravity wave scale. The estimated maximum cloud lifetime of around 3–4 days for cirrus clouds above 15 km induced by deep convection seems to be large and could have an impact on the radiation budget of clouds as well as for heterogeneous chemical processes at the tropopause region.

[58] Further investigations are necessary in a similar manner outlined at the end of section 6.5. The combination of different CRISTA observations, convectively generated gravity waves, water vapor measurements below and above the tropopause [*Offermann et al.*, 2002], in conjunction with other satellite data sets (e.g., precipitation, cloud coverage) and in situ temperature measurements by radiosondes could contribute to the understanding of formation and persistence of cirrus clouds around the tropical tropopause.

[59] **Acknowledgments.** The authors wish to thank Julio Bacmeister (GSFC) for the trajectory program and R. Rood (GSFC) for the DAO meteorological analyses. The authors would also like to thank Marion Legg (NASA/Ames) and Matthias Donner (Wuppertal) for the preparation of the GOES/GMS data set and the trajectory statistics, respectively. P.-H. Wang is supported by NASA contract NAS1-99129. The CRISTA project is funded by the Bundesministerium für Bildung und Forschung through the Deutsches Zentrum für Luft- und Raumfahrt e.V. (DLR) under project number 50 QV 9802 4. The CRISTA instrument was flown by NASA on the Space Shuttle missions STS66 and STS85.

References

Ackerman, T. P., K. N. Liou, F. P. J. Valero, and L. Pfister, Heating rates in tropical anvils, *J. Atmos. Sci.*, *45*, 1606–1623, 1988.

Bacmeister, J. T., V. Kuell, D. Offermann, M. Riese, and J. W. Elkins, Intercomparison of satellite and aircraft observations of ozone, CFC-11, and NO_y using trajectory mapping, *J. Geophys. Res.*, *104*, 16,379–16,390, 1999.

Borrmann, S., S. Solomon, J. E. Dye, and B. Luo, The potential of cirrus clouds for heterogeneous chlorine activation, *Geophys. Res. Lett.*, *23*, 2133–2136, 1996.

Danielsen, E. F., In situ evidence of rapid, vertical irreversible transport of lower tropospheric air into the lower stratosphere by convective cloud turrets and by large-scale upwelling in tropical cyclones, *J. Geophys. Res.*, *98*, 8665–8681, 1993.

Grossmann, K. U., Recent improvements in middle atmosphere remote sounding techniques: The CRISTA-SPAS experiment, *Geophys. Monogr.*, *123*, 287–304, 2000.

Grossmann, K. U., D. Offermann, O. Gusev, J. Oberheide, M. Riese, and R. Spang, The CRISTA-2 mission, *J. Geophys. Res.*, in press, 2002.

Hervig, M. E., and M. McHugh, Cirrus detection using HALOE measurements, *Geophys. Res. Lett.*, *26*, 719–722, 1999.

Houze, R. A., Observed structure of the mesoscale convective systems and implications for large scale heating, *Q. J. R. Meteorol. Soc.*, *115*, 425–461, 1989.

Jensen, E. J., S. Kinne, and O. B. Toon, Tropical cirrus cloud radiative forcing: Sensitivity studies, *Geophys. Res. Lett.*, *21*, 2023–2026, 1994.

Jensen, E. J., O. B. Toon, H. B. Selkirk, J. D. Spinhirne, and M. R. Schoeberl, On the formation and persistence of subvisible cirrus clouds near the tropical tropopause, *J. Geophys. Res.*, *101*, 21,361–21,375, 1996a.

Jensen, E. J., O. B. Toon, L. Pfister, and H. B. Selkrik, Dehydration of the upper troposphere and lower stratosphere by subvisible cirrus clouds near the tropical tropopause, *Geophys. Res. Lett.*, *23*, 825–828, 1996b.

Kent, G. S., D. M. Winker, M. A. Vaughan, P.-H. Wang, and K. M. Skeens, Simulations of Stratospheric Aerosol and Gas Experiment (SAGE) II cloud measurements using airborne lidar data, *J. Geophys. Res.*, *105*, 21,795–21,807, 1997.

Liao, X., W. B. Rossow, and D. Rind, Comparison between SAGE II and ISCCP high-level clouds, 1, Global and zonal mean cloud amounts, *J. Geophys. Res.*, *100*, 1121–1135, 1995.

Liebmann, B., and C. A. Smith, Description of a complete (interpolated) outgoing longwave radiation dataset, *Bull. Am. Meteorol. Soc.*, *77*, 1275–1277, 1996.

Liou, K. N., S. C. Ou, Y. Takano, F. P. Valero, and T. P. Ackerman, Remote sounding of tropical cirrus cloud temperatures and optical depth using 6 micron and 10.6 micron radiometers during STEP, *J. Appl. Meteorol.*, *29*, 716–726, 1990.

Marti, J., and K. Mauersberger, A survey and new measurements of ice vapor pressure at temperatures between 170 and 250 K, *Geophys. Res. Lett.*, *20*, 363–366, 1993.

Massie, S., P. Lowe, X. Tie, M. Hervig, G. Thomas, and J. Russell III, Effect of the 1997 El Niño on the distribution of upper tropospheric cirrus, *J. Geophys. Res.*, *105*, 22,725–22,741, 2000.

McLandress, C., M. J. Alexander, and D. L. Wu, Microwave Limb Sounder observations of gravity waves in the stratosphere: A climatology and interpretation, *J. Geophys. Res.*, *105*, 11,947–11,967, 2000.

Mergenthaler, J. L., A. E. Roche, J. B. Kumer, and G. A. Ely, Cryogenic Limb Array Etalon Spectrometer observations of tropical cirrus, *J. Geophys. Res.*, *104*, 22,183–22,194, 1999.

Mote, P. W., K. H. Rosenlof, M. E. McIntyre, E. S. Carr, J. C. Gille, J. R. Holton, J. S. Kinnersley, H. C. Pumphrey, J. M. Russell III, and J. W. Waters, An atmospheric tape recorder: The imprint of the tropical tropopause temperature on the stratospheric water vapor, *J. Geophys. Res.*, *101*, 3989–4006, 1996.

Offermann, D., K. U. Grossmann, P. Barthol, P. Knieling, M. Riese, and R. Trant, The CRyogenic Infrared Spectrometers and Telescopes for the Atmosphere (CRISTA) experiment and middle atmosphere variability, *J. Geophys. Res.*, *104*, 16,311–16,325, 1999.

Offermann, D., B. Schaeler, M. Riese, M. Langfermann, M. Jarisch, G. Eidmann, C. Schiller, H. G. J. Smit, and W. G. Read, Water vapor at the tropopause during the CRISTA 2 mission, *J. Geophys. Res.*, *107*, doi:10.1029/2001JD000700, in press, 2002.

Pawson, S., and M. Fiorino, A comparison of reanalyses in the tropical stratosphere, part 3, inclusion of the pre-satellite data era, *Clim. Dyn.*, *15*(4), 241–250, 1999.

Pfister, L., et al., Aircraft observations of thin cirrus clouds near the tropical tropopause, *J. Geophys. Res.*, *106*, 9765–9786, 2001.

Prabhakara, C., D. P. Kratz, Y.-M. Yoo, G. Dalu, and A. Vernekar, Optically thin cirrus clouds: Radiative impact on the warm pool, *J. Quant. Spectrosc. Radiat. Transfer*, *49*, 467–483, 1993.

Preusse, P., G. Eidmann, S. D. Eckermann, B. Schaeler, R. Spang, and D. Offermann, Convectively generated gravity waves as seen in the CRISTA temperatures, *Adv. Space Res.*, in press, 2001.

Remedios, J. J., Extreme atmospheric constituent profiles for MIPAS, in *Proceedings of the European Symposium on Atmospheric Measurements from Space, 20–22 January*, Vol. 2, pp. 779–783, ESTEC, Nordwijk, Netherlands, 1999.

Reid, G. C., and K. S. Gage, The tropical tropopause over the western Pacific: Wave driving, convection, and the annual cycle, *J. Geophys. Res.*, *101*, 21,233–21,241, 1996.

Reid, G. C., and K. S. Gage, On the annual variations in the height of the tropical tropopause, *J. Atmos. Sci.*, *38*, 5629–5635, 1981.

Riese, M., R. Spang, P. Preusse, M. Ern, M. Jarisch, D. Offermann, and K. U. Grossmann, Cryogenic Infrared Spectrometers and Telescopes for the Atmosphere (CRISTA) data processing and atmospheric temperature and trace gas retrieval, *J. Geophys. Res.*, *104*, 16,349–16,367, 1999a.

Riese, M., X. Tie, G. Brasseur, and D. Offermann, Three-dimensional simulation of stratospheric trace gas distributions measured by CRISTA, *J. Geophys. Res.*, *104*, 16,419–16,435, 1999b.

Salby, M. L., and H. H. Hendon, Intraseasonal behavior of clouds, temperature, and motion in the tropics, *J. Atmos. Sci.*, *51*, 2207–2224, 1994.

Sassen, K., and B. S. Cho, Subvisual-thin cirrus clouds lidar data set for satellite verification and climatological research, *J. Appl. Meteorol.*, *31*, 1275–1285, 1992.

Sassen, K., M. K. Griffin, and G. C. Dodd, Optical scattering and microphysical properties of subvisible cirrus clouds, and climatic implications, *J. Appl. Meteorol.*, *28*, 91–98, 1989.

Sherwood, S. C., On moistening of the tropical troposphere by cirrus clouds, *J. Geophys. Res.*, *104*, 11,949–11,960, 1999.

Sherwood, S. C., and A. E. Dessler, On the control of stratospheric humidity, *Geophys. Res. Lett.*, *27*, 2513–2516, 2000.

Schubert, S. D., R. Rood, and J. Pfaendtner, An assimilated dataset for Earth Science Applications, *Bull. Am. Meteorol. Soc.*, *74*, 2331–2342, 1993.

Smith, A. K., P. Preusse, and J. Oberheide, Middle atmosphere Kelvin waves observed in CRISTA 1 and 2 temperature and trace species, *J. Geophys. Res.*, *107*, doi:10.1029/2001JD000700, in press, 2002.

Solomon, S., S. Borrmann, R. R. Gracia, R. Protmann, L. Thomason, L. R. Poole, D. Winker, and P. M. McCormick, Heterogeneous chlorine chemistry in the tropopause region, *J. Geophys. Res.*, *102*, 21,411–21,429, 1997.

Spang, R., M. Riese, and D. Offermann, CFC11 measurements by CRISTA, *Adv. Space. Res.*, *19*, 575–578, 1997.

Spang, R., M. Riese, and D. Offermann, CRISTA-2 observations of the south polar vortex in winter 1997: A new dataset for polar process studies, *Geophys. Res. Lett.*, *28*, 3159–3163, 2001.

Thomason, L. W., and L. R. Poole, A SAGE look at three periods of low stratospheric aerosol loading: 1979, 1989–1990, and 1998–1999, *Eos Trans. AGU*, *80*(16), November 16 1999.

Wackerly, D. D., W. M. Mendenhall III, and R. L. Schaeffer, *Mathematical Statistics with Applications*, Fifth Edition, Duxbury, 1996.

Wang, P. H., M. P. McCormick, L. R. Poole, W. P. Chu, G. K. Yue, G. S. Kent, and K. S. Skeens, Tropical high cloud characteristics derived from SAGE II extinction measurements, *Atmos. Res.*, *34*, 53–83, 1994.

Wang, P. H., P. Minnis, M. P. McCormick, G. S. Kent, and K. S. Skeens, A 6-year climatology of cloud occurrence frequency from SAGE II observations (1985–1990), *J. Geophys. Res.*, *101*, 29,407–29,429, 1996.

Wallace, J. M., E. M. Rasmusson, T. P. Mitchell, V. E. Kousky, E. S. Sarachik, and H. von Stroch, On the structure and evolution of ENSO-related climate variability in the tropical Pacific: Lessons from TOGA, *J. Geophys. Res.*, *103*, 14,241–14,259, 1998.

Weaver, C. P., W. D. Collins, and H. Grassl, Relationship between clear-sky atmospheric greenhouse effect and deep convection during the Central Pacific Experiment: Model calculations and satellite observations, *J. Geophys. Res.*, *99*, 25,891–25,901, 1998.

Winker, D. W., and C. R. Trepte, Laminar cirrus observed near the tropical tropopause by LITE, *Geophys. Res. Lett.*, *25*, 3351–3354, 1998.

R. Spang, EOS, Space Research Centre, University of Leicester, University Road, Leicester, LE1 7RH, England. (r.spang@le.ac.uk)

G. Eidmann, D. Offermann, P. Preusse, and M. Riese, University of Wuppertal, Gauss Str. 20, 42097 Wuppertal, Germany.

L. Pfister, NASA/Ames Research Center, MS 245-5, Hampton, VA 23691-2199, USA.

P.-H. Wang, Science and Technology Corporation, 101 Research Drive, Hampton, VA 23666-1340, USA.